

Chemical dynamics simulations of the monohydrated $\text{OH}^-(\text{H}_2\text{O}) + \text{CH}_3\text{I}$ reaction. Atomic-level mechanisms and comparison with experiment

Cite as: J. Chem. Phys. **142**, 244308 (2015); <https://doi.org/10.1063/1.4922451>

Submitted: 15 March 2015 . Accepted: 02 June 2015 . Published Online: 25 June 2015

Jing Xie, Rico Otto, Roland Wester, and William L. Hase



View Online



Export Citation



CrossMark

ARTICLES YOU MAY BE INTERESTED IN

[Nucleophilic substitution with two reactive centers: The \$\text{CN}^- + \text{CH}_3\text{I}\$ case](#)

The Journal of Chemical Physics **143**, 184309 (2015); <https://doi.org/10.1063/1.4934993>

[\$\text{NH}_2^-\$ in a cold ion trap with He buffer gas: Ab initio quantum modeling of the interaction potential and of state-changing multichannel dynamics](#)

The Journal of Chemical Physics **148**, 184305 (2018); <https://doi.org/10.1063/1.5022633>

[Photochemistry and spectroscopy of small hydrated magnesium clusters \$\text{Mg}^+\(\text{H}_2\text{O}\)_n\$, \$n = 1-5\$](#)

The Journal of Chemical Physics **149**, 044309 (2018); <https://doi.org/10.1063/1.5037401>



Lock-in Amplifiers



Zurich
Instruments

Watch the Video ▶

Chemical dynamics simulations of the monohydrated OH⁻(H₂O) + CH₃I reaction. Atomic-level mechanisms and comparison with experiment

Jing Xie,¹ Rico Otto,² Roland Wester,³ and William L. Hase^{1,a)}

¹Department of Chemistry and Biochemistry, Texas Tech University, Lubbock, Texas 79409-1061, USA

²Department of Chemistry and Biochemistry, University of California, San Diego, 9500 Gilman Drive, La Jolla, California 92093, USA

³Institut für Ionenphysik und Angewandte Physik, Universität Innsbruck, Technikerstraße 25/3, A-6020 Innsbruck, Austria

(Received 15 March 2015; accepted 2 June 2015; published online 25 June 2015)

Direct dynamics simulations, with B97-1/ECP/d theory, were performed to study the role of microsolvation for the OH⁻(H₂O) + CH₃I reaction. The S_N2 reaction dominates at all reactant collision energies, but at higher collision energies proton transfer to form CH₂I⁻, and to a lesser extent CH₂I⁻(H₂O), becomes important. The S_N2 reaction occurs by direct rebound and stripping mechanisms, and 28 different indirect atomistic mechanisms, with the latter dominating. Important components of the indirect mechanisms are the roundabout and formation of S_N2 and proton transfer pre-reaction complexes and intermediates, including [CH₃-I--OH]⁻. In contrast, for the unsolvated OH⁻ + CH₃I S_N2 reaction, there are only seven indirect atomistic mechanisms and the direct mechanisms dominate. Overall, the simulation results for the OH⁻(H₂O) + CH₃I S_N2 reaction are in good agreement with experiment with respect to reaction rate constant, product branching ratio, etc. Differences between simulation and experiment are present for the S_N2 velocity scattering angle at high collision energies and the proton transfer probability at low collision energies. Equilibrium solvation by the H₂O molecule is unimportant. The S_N2 reaction is dominated by events in which H₂O leaves the reactive system as CH₃OH is formed or before CH₃OH formation. Formation of solvated products is unimportant and participation of the (H₂O)CH₃OH---I⁻ post-reaction complex for the S_N2 reaction is negligible. © 2015 AIP Publishing LLC. [<http://dx.doi.org/10.1063/1.4922451>]

I. INTRODUCTION

Reaction rates, for X⁻ + CH₃Y → XCH₃ + Y⁻ S_N2 reactions with barriers, are often orders of magnitude smaller in aqueous solution than in the gas phase.^{1–4} Water molecules solvate the X⁻ + CH₃Y reactants more strongly than the [X---CH₃---Y]⁻ S_N2 transition state (TS), substantially raising the barrier for reaction in solution.^{2,5} Non-equilibrium barrier recrossing effects may be important for S_N2 reactions in both the gas phase^{6–8} and in solution,^{9,10} but they are less important than the preferential solvation of the reactants in aqueous solution. Both theoretical models^{11,12} and molecular dynamics simulations¹⁰ have been used to investigate the possible importance of non-equilibrium solvation for S_N2 reactions in water.

Less well understood is the role of solvation for barrierless, exothermic X⁻ + CH₃Y reactions. Of particular interest is the extent of equilibration between the reactive system and the water solvent as potential energy is released during the reaction. Understanding the extent of equilibration is important for characterizing possible roles of potential energy minima for the reaction.^{13,14} If the X⁻ + CH₃Y reaction has pathways in addition to the S_N2 pathway, any equilibration of the potential energy release is expected to affect the branching ratio between these pathways. The Cl⁻ + CH₃Br S_N2 reaction has a barrier in water, but is exothermic, and its dynamics in water and with

microsolvation have been studied by direct dynamics simulations.^{15,16} Binding of the halogen ions to the water molecules and the role of the water molecules in suppressing the reaction rate were considered.

The OH⁻ + CH₃I → CH₃OH + I⁻ S_N2 reaction is barrierless, highly exothermic, and there are additional reaction pathways; e.g., the proton transfer products H₂O + CH₂I⁻. The role of solvation on the dynamics of the OH⁻ + CH₃I reaction has been investigated by crossed molecular beam, ion-imaging experiments^{17–19} of the microsolvated reactants OH⁻(H₂O)_{1,2} + CH₃I, and important differences were found between the reaction dynamics of “bare” OH⁻ and singly and doubly hydrated OH⁻. Additional experiments have been performed to study the chemical kinetics for reactions of hydrated OH⁻ with CH₃Cl and CH₃Br.^{1,3,20–23} Direct chemical dynamics simulations have provided detailed atomistic information regarding the dynamics of the OH⁻ + CH₃I reaction, including comparison with experiment,^{24,25} and a preliminary report has presented simulations and comparisons with experiment for the mono-hydrated OH⁻(H₂O) + CH₃I reaction.¹⁷ This work indicates the atomistic motion of the H₂O molecule is different for the OH⁻(H₂O) + CH₃I reaction than for the OH⁻(H₂O) + CH₃Cl reactions.²⁶ A particularly interesting issue is the extent to which the H₂O molecule may “align” OH⁻ in the entrance channel to facilitate the S_N2 reaction.^{5,18}

In this article, extensive direct chemical dynamics simulations are reported for the OH⁻(H₂O) + CH₃I reaction, to

^{a)}E-mail: bill.hase@ttu.edu

compare with experiment and provide insight into the reaction's atomic-level dynamics. Of interest is to establish possible connections between gas-phase and solution kinetics, and understand how a single water molecule may affect chemical reaction dynamics.^{18,27}

II. COMPUTATIONAL METHOD

A. Electronic structure calculations

The NWChem²⁸ computer program was used to perform the electronic structure calculations. In previous work, density functional theory (DFT)²⁹ with the B97-1^{30,31} functional was used to characterize the potential energy surface (PES) for the OH⁻ + CH₃I reaction. Stationary points were identified and their structures, vibrational frequencies, and energies determined. The basis set used for the calculations is called effective core potential (ECP)/d,³² for which Dunning and Woon's aug-cc-PVDZ basis set^{33,34} is used for the H, C, and O atoms. For iodine, the Wadt and Hay ECP³⁵ was used for the core electrons and a 3s, 3p basis set was used for the valence electrons, which was augmented by a d-polarization function with a 0.262 exponent, and s, p, and d diffuse functions with exponents of 0.034, 0.039, and 0.0873, respectively.³⁶ In previous studies,^{17,24} the B97-1/ECP/d method was found to give overall reaction energies in good agreement with experiment. This method was also used in direct dynamics simulations of the OH⁻ + CH₃I reaction and good agreement was obtained with the experimental anion product ratios, product energy partitioning, and rate constants.^{24,25} Given the overall previous success of the B97-1/ECP/d method for the OH⁻ + CH₃I reaction, this method was selected for the OH⁻(H₂O) + CH₃I direct dynamics simulations reported here.

B. Direct dynamics simulations

The direct dynamics simulations were performed with the VENUS/NWChem software package,³⁷ for which the VENUS chemical dynamics computer program^{38,39} is interfaced with NWChem.²⁸ To directly compare with the experiments of the Wester research group,^{17–19} initial conditions for the trajectories were selected for collision energies (i.e., reagent relative translational energy) E_{rel} of 0.05, 0.5, 1.0, and 2.0 eV, CH₃I vibrational and rotational temperatures of $T_v = 330$ K and $T_r = 130$ K, and a OH⁻(H₂O) vibrational and rotational temperature of 100 K. The CH₃I and OH⁻(H₂O) vibrational and rotational energies were sampled from their Boltzmann distributions. Quasiclassical sampling⁴⁰ was used to transform these energies to the Cartesian coordinates and momenta used for the trajectories. With this sampling, the vibrational modes of the reactant molecules have random phases. CH₃I and OH⁻(H₂O) had random orientations, and the initial OH⁻(H₂O) + CH₃I center-of-mass separation was set at 8.5–12.0 Å. Algorithms for sampling the OH⁻(H₂O) + CH₃I initial conditions are standard options in VENUS and have been described previously.⁴⁰

Vibrational energies for the OH⁻(H₂O) initial conditions are those for one of the two potential energy minima for the proton transfer double-well potential; i.e., HO⁻—HOH \leftrightarrow HOH—OH⁻. This initial condition model approximates the

OH⁻(H₂O) vibrational energy levels, since the barrier for proton transfer is quite low and the transferring proton is delocalized between the two O-atoms.^{41–43} From a quantum mechanical calculation, using a CCSD(T) potential energy curve, the zero-point level of the double-well potential is 1.24 kcal/mol as compared to the proton transfer barrier of only 0.20 kcal/mol.⁴³ For the OH⁻(H₂O) potential energy minimum, the comparison zero-point energy (ZPE) is that for the OH* stretch of the transferring H-atom; i.e., HOH*—OH⁻. This ZPE, for the B97-1/ECP/d method used for the simulations is 1.68 kcal/mol and the proton transfer barrier is 0.06 kcal/mol.

There is a substantial delocalization of the transferring proton in the initial conditions for OH⁻(H₂O). As discussed above, initial conditions are chosen for the vibrational modes of one of the OH⁻(H₂O) potential energy minima but, because of the low barrier for proton transfer, ~20% of the initial conditions transfer the proton to the other potential energy minimum. In addition, there is substantial proton transfer between the two potential energy minima as OH⁻(H₂O) and CH₃I collide. Figure 1 depicts for 1000 fs the typical atomic-level motion for a trajectory initiated with ZPE in each of the OH⁻(H₂O) vibrational modes. There is continual proton transfer between the two O-atoms. During the average time it takes OH⁻(H₂O) and CH₃I to collide from their initial separation, i.e., ~150 fs at $E_{rel} = 2.0$ eV and ~700 fs at $E_{rel} = 0.05$ eV, there are numerous proton transfers between the two minima.

McCoy *et al.*⁴⁴ have used a high-level, full dimensional PES and diffusion Monte Carlo quantum calculations to determine vibrational energy levels for OH⁻(H₂O). Of particular interest for the current study is their finding that the ground state vibrational density is a maximum at the saddle point between the two minima for the transferring proton. Another approach for choosing initial conditions for the trajectories would be to first transform the OH⁻(H₂O) vibrational and rotational energies to Cartesian coordinates at this saddle point and then integrate the OH⁻(H₂O) motion for a random time within one complete classical period for the transferring proton's motion. In this manner, a random phase is chosen for

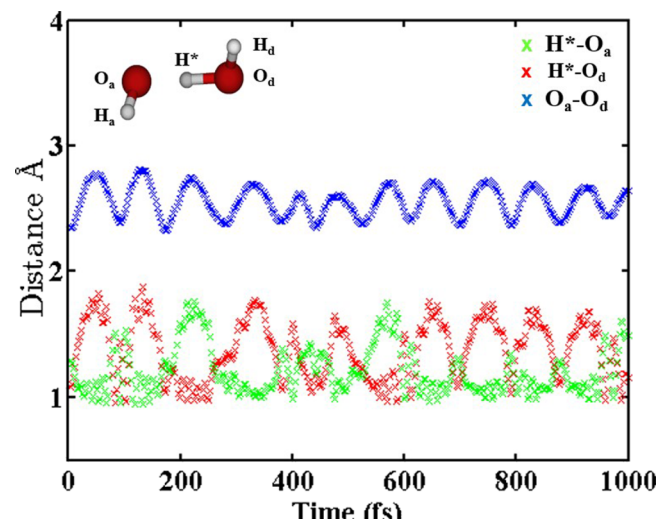


FIG. 1. Distances between the sharing H* atom and O atoms for a trajectory initiated at a OH⁻(H₂O) minimum. H* stands for the sharing H atom and “a” for acceptor and “d” for donor.

the motion of the transferring proton, so that the trajectory results are independent of the initial separation between the two reactants.^{40,45} It is expected that this sampling algorithm will give the same dynamics as the one used here and described above. Noteworthy is that the OH⁻(H₂O) ZPE is 6760 cm⁻¹ for the sampling procedure used here, as compared to the 6605 cm⁻¹ determined by McCoy *et al.*⁴⁴

A sixth-order symplectic algorithm^{46,47} with a 2.5 fs time step was used to integrate the trajectories; i.e., the same method as used for the OH⁻ + CH₃I simulations.^{17,24,25} The total integration time depended on the collision energy; i.e., 4.0–9.0 ps for 0.05 eV, 1.5–6.0 ps for 0.5 eV, 1.0–4.0 ps for 1.0 eV, and 0.5–2.5 ps for 2.0 eV. Reactive trajectories were identified by viewing their animations and, thus, determining their atomic-level mechanisms.

Properties determined from the simulations are the reaction pathways and their atomic-level mechanisms, reaction cross sections for the different pathways and the overall reaction rate constant, velocity scattering angle distribution for the OH⁻(H₂O) + CH₃I → CH₃OH + I⁻ + H₂O S_{N2} reaction, and distribution of the pseudo internal energy *p*-E_{int} for the S_{N2} products CH₃OH + H₂O in their center-of-mass frame. (The *p*-E_{int} energy is the total energy available to the reaction products, minus the relative translational energy between I⁻ and CH₃OH + H₂O. The ZPE of CH₃OH + H₂O is removed in calculating *p*-E_{int}). The simulation properties compared with experiment are the relative product ion yields, overall reaction rate constant, collision-induced dissociation (CID) cross section, and the S_{N2} velocity scattering angle and *p*-E_{int} distributions.

III. PROPERTIES OF THE POTENTIAL ENERGY SURFACE

A. Stationary point structures and energies for the different reaction paths

The B97-1/ECP/d method was used to calculate energies for the OH⁻(H₂O) + CH₃I reaction pathways. Eleven product

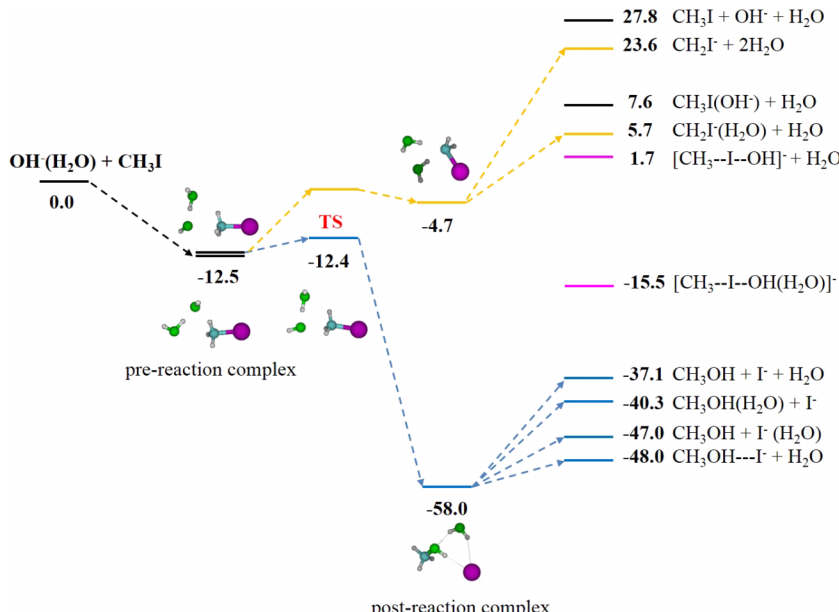


TABLE I. Reaction enthalpies for different OH⁻(H₂O) + CH₃I product channels.^a

Products	ΔH_{rxn} (kcal/mol)	
	0 K	B97-1 ^b
I ⁻ (CH ₃ OH)(H ₂ O)		-58.0(-63.9)
I ⁻ (CH ₃ OH)		-48.0(-51.8)
CH ₃ OH + I ⁻ (H ₂ O)	-48.4 ± 2.5	-47.0(-51.4)
CH ₃ OH(H ₂ O) + I ⁻		-40.3(-45.5)
CH ₃ OH + I ⁻ + H ₂ O	-36.9 ± 2.5	-37.1(-40.5)
[CH ₃ --I-OH] ⁻ (H ₂ O)		-15.5(-18.0)
[CH ₃ --I-OH] ⁻ + H ₂ O		1.7(1.5)
CH ₂ I ⁻ (H ₂ O) + H ₂ O ^c		5.7(5.8)
CH ₃ I(OH ⁻) + H ₂ O ^c		7.5(8.3)
CH ₂ I ⁻ + 2H ₂ O	23.1 ± 2.8	23.6(25.5)
CH ₃ I + OH ⁻ + H ₂ O	28.8 ^b ± 6.9	27.8(28.3)

^aEnthalpies of reaction ΔH_{rxn} calculated from enthalpies of formation of ΔH_f^0 at 0 K^{48,49} for the I⁻ and CH₂I⁻ product channels. The OH⁻(H₂O) binding energy is taken from Ref. 46.

^bValues including zero point energy are in normal text, and values without zero point energy are in parentheses.

^cAs discussed in Sec. III B 2, the structures for CH₂I⁻(H₂O) and CH₃I(OH⁻) are HOH---CH₂I⁻ and HO---HCH₂I, respectively.

channels were observed at the termination of the trajectories: i.e., CH₃OH + I⁻ + H₂O, CH₃OH + I⁻(H₂O), CH₃OH(H₂O) + I⁻, I⁻(CH₃OH) + H₂O, I⁻(CH₃OH)(H₂O), CH₂I⁻ + 2H₂O, CH₂I⁻(H₂O) + H₂O, [CH₃--I-OH]⁻ + H₂O, [CH₃--I-OH]⁻(H₂O), CH₃I(OH⁻) + H₂O, and CH₃I + OH⁻ + H₂O. Reaction energies for all of these pathways are summarized in Table I, and the energies for ten of the pathways are depicted in Figure 2. There is good agreement between the experimental^{48–50} and DFT energies for all the pathways for which experimental energies are available. The proton transfer reactions become endothermic with the H₂O molecule added; e.g., the B97-1/ECP/d reaction energy with ZPE included is -4.7 kcal/mol for OH⁻ + CH₃I → CH₂I⁻ + H₂O, but 23.6 kcal/mol for OH⁻(H₂O) + CH₃I → CH₂I⁻ + 2H₂O.

Stationary point energies and structures for the OH⁻(H₂O) + CH₃I → CH₃OH + I⁻ + H₂O S_{N2} pathway are given

FIG. 2. Schematic energy profile for the OH⁻(H₂O) + CH₃I → CH₃OH + I⁻ + H₂O S_{N2} reaction, and other pathways, at the DFT/B97-1/ECP/d level of theory. The energies shown are in kcal/mol and are relative to the OH⁻(H₂O) + CH₃I reactants. Zero point energies are included. The TS was not found which connects the proton transfer pre- and post-reaction complexes, (H₂O)HO⁻---HCH₂I and CH₂I⁻---H₂O(H₂O); see discussion in the text.

in Figure 2. Two structures were found for the pre-reaction complex, with the upper structure (denoted as A1) only 0.08 kcal/mol higher in energy than the lower structure (denoted as A2). If the H₂O molecule is removed from A2, the resulting structure is similar to that of the hydrogen-bonded pre-reaction complex for the OH⁻ + CH₃I → CH₃OH + I⁻ reaction.²⁴ For A1 the O---C-I angle is 172.1°, resulting in a nearly linear structure for the HO⁻---CH₃I heavy atoms, with OH⁻ attacking the backside of CH₃I as for a traditional S_N2 reaction.^{51,52} This linear structure was not found for the OH⁻ + CH₃I → CH₃OH + I⁻ reaction.²⁴ This difference in the structures of the pre-reaction complexes for the OH⁻ + CH₃I and OH⁻(H₂O) + CH₃I S_N2 reactions has been discussed by Otto and Wester.²⁷

The S_N2 TS has an energy only 0.1 kcal/mol higher than that of the pre-reaction complexes. The structure of the TS is very similar to that of the pre-reaction complex A2, where the major difference is for the angle O---C-I which is 150.8° for the TS as compared to 172.1° for the complex. For the post-reaction complex, there are two structures with similar energies. As shown in Figures 2 and 3, the S_N2 and proton transfer pathways have the same pre-reaction complex, (H₂O)HO⁻---HCH₂I, but different post-reaction complexes. Multiple unsuccessful attempts were made to determine the structure for the TS connecting the proton transfer pre- and post-reaction complexes, (H₂O)HO⁻---HCH₂I and CH₂I⁻---H₂O(H₂O), respectively, in Figure 2. A scan involving the transferring proton gives a very small barrier, as shown in the supplementary material Fig. S1,⁵³ but the TS could not be found. The direct dynamics simulations provide insights into the roles of the above complexes and TSs in the atomistic reaction mechanisms.

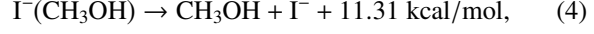
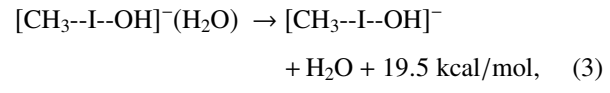
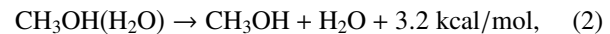
B. Product complexes

Eight complexes are formed at the termination of the trajectories; i.e., I⁻(H₂O), CH₃OH(H₂O), I⁻(CH₃OH),

I⁻(CH₃OH)(H₂O), CH₂I⁻(H₂O), CH₃I(OH⁻), [CH₃--I--OH]⁻, and [CH₃--I--OH]⁻(H₂O). I⁻(H₂O), CH₃OH(H₂O), I⁻(CH₃OH)(H₂O), and [CH₃--I--OH]⁻(H₂O) are hydrated complexes, and given sufficient energy will dissociate losing H₂O. The remaining four complexes have the same mass to charge ratio and their dynamics are overall more complicated than those for the above hydrated complexes. The internal energies of the product complexes were calculated; and if the energy was larger than the threshold energy to form products with ZPE, it was assumed the complex would dissociate. This threshold energy is (E_{dis} + ZPE), where E_{dis} is the classical dissociation energy and ZPE is the zero-point energy of the products. [CH₃--I--OH]⁻, CH₂I⁻(H₂O), and CH₃I(OH⁻) complexes have multiple dissociation pathways and, as described below, direct dynamics simulations were performed to determine the branching between these pathways.

1. I⁻(H₂O), CH₃OH(H₂O), [CH₃--I--OH]⁻(H₂O), and I⁻(CH₃OH) complexes

The three hydrated complexes I⁻(H₂O), CH₃OH(H₂O), and [CH₃--I--OH]⁻(H₂O) may dissociate by losing the H₂O molecule, and I⁻(CH₃OH) may dissociate to CH₃OH + I⁻,



where ZPEs are not included in the reaction energies. Whether these complexes, existing at the end of a trajectory, will ultimately dissociate is determined by comparing their internal and dissociation energies as described above.

Only a few of the I⁻(H₂O) complexes dissociate at the collision energies of 2.0 and 1.0 eV. For all of the trajectories at 0.5

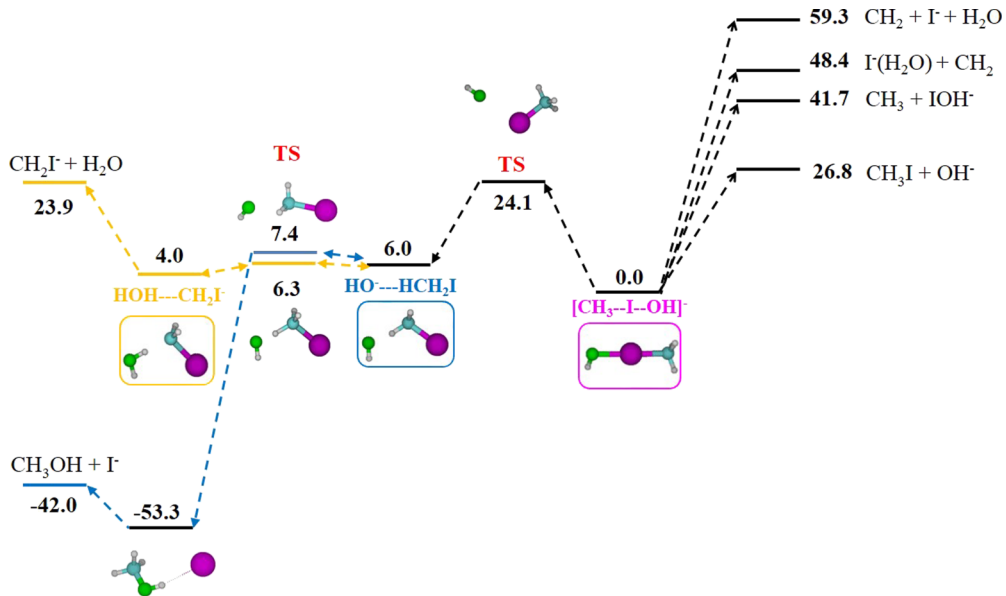


FIG. 3. Schematic energy profile for dissociation of [CH₃--I--OH]⁻ to CH₂I⁻ + H₂O and CH₃OH + I⁻ at the DFT/B97-1/ECP/d level of theory. Energies shown are in kcal/mol and relative to the [CH₃--I--OH]⁻ ion-molecule complex. Zero point energies are included.

and 0.05 eV, there is no dissociation of the remaining $\text{I}^-(\text{H}_2\text{O})$ complexes. All of the $\text{CH}_3\text{OH}(\text{H}_2\text{O})$ and $[\text{CH}_3-\text{I}-\text{OH}]^-(\text{H}_2\text{O})$ complexes dissociated. Very little of $\text{I}^-(\text{CH}_3\text{OH})$ remained undissociated.

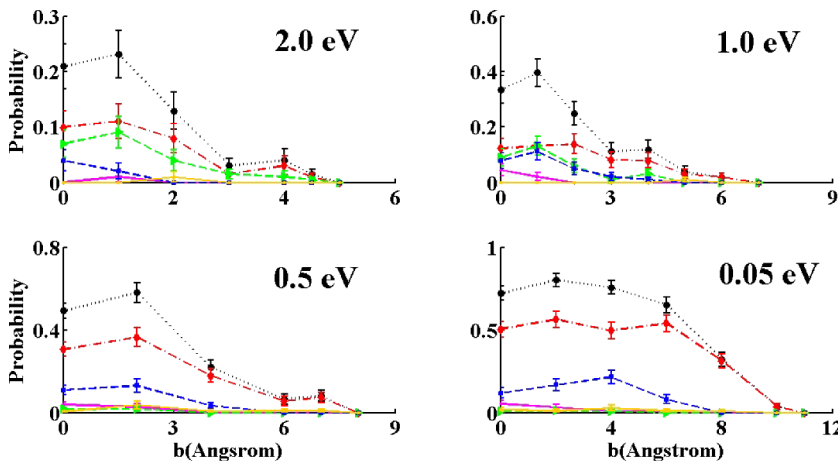
2. $\text{CH}_2\text{I}^-(\text{H}_2\text{O})$, $\text{CH}_3\text{I}(\text{OH}^-)$, and $[\text{CH}_3-\text{I}-\text{OH}]^-$ complexes

It is critical to study the dissociation of the three complexes $\text{CH}_2\text{I}^-(\text{H}_2\text{O})$, $\text{CH}_3\text{I}(\text{OH}^-)$, and $[\text{CH}_3-\text{I}-\text{OH}]^-$, since they have the same mass-charge ratio and mass spectrometry experiments cannot distinguish them.

According to previous calculations^{24,25} for the $\text{OH}^- + \text{CH}_3\text{I}$ reaction and as shown in Figure 3, accurate structural expressions for $\text{CH}_2\text{I}^-(\text{H}_2\text{O})$ and $\text{CH}_3\text{I}(\text{OH}^-)$ are $\text{HOH---CH}_2\text{I}^-$ and $\text{HO}^- --- \text{HCH}_2\text{I}$, respectively. $\text{HO}^- --- \text{HCH}_2\text{I}$ is a pre-reaction complex on the PES for both the $\text{S}_{\text{N}}2$, $\text{OH}^- + \text{CH}_3\text{I} \rightarrow \text{CH}_3\text{OH} + \text{I}^-$, and proton transfer, $\text{OH}^- + \text{CH}_3\text{I} \rightarrow \text{CH}_2\text{I}^- + \text{H}_2\text{O}$, pathways and $\text{HOH---CH}_2\text{I}^-$ is a post-reaction complex for the proton transfer pathway. Considering the low barrier of only 2.73 kcal/mol between the pre-reaction complex $\text{HO}^- --- \text{HCH}_2\text{I}$ and post-reaction complex $\text{HOH---CH}_2\text{I}^-$, both complexes are possible intermediates for forming the $\text{CH}_2\text{I}^- + \text{H}_2\text{O}$ and $\text{CH}_3\text{OH} + \text{I}^-$ products. These complexes couple the $\text{S}_{\text{N}}2$ and proton transfer pathways.

With ZPE included, the barrier for $\text{HO}^- --- \text{HCH}_2\text{I}$ dissociating to $\text{CH}_3\text{OH} + \text{I}^-$ is 29.7 kcal/mol, and to $\text{CH}_2\text{I}^- + \text{H}_2\text{O}$ is 43.9 kcal/mol. The barrier for $\text{HOH---CH}_2\text{I}^-$ dissociating to $\text{CH}_3\text{OH} + \text{I}^-$ is 32.2 kcal/mol, and to $\text{CH}_2\text{I}^- + \text{H}_2\text{O}$ is 46.3 kcal/mol. When the trajectories were terminated, the total energy of the $\text{HO}^- --- \text{HCH}_2\text{I}$ and $\text{HOH---CH}_2\text{I}^-$ complexes did not exceed 40 kcal/mol, thus, these two complexes only dissociated to $\text{CH}_3\text{OH} + \text{I}^-$.

Dissociation of $[\text{CH}_3-\text{I}-\text{OH}]^-$ is more complex because of the multiple product pathways, i.e., $\text{CH}_3\text{I} + \text{OH}^-$, $\text{CH}_2\text{I}^- + \text{H}_2\text{O}$, $\text{CH}_3\text{OH} + \text{I}^-$, $\text{CH}_3 + \text{IOH}^-$, and $\text{CH}_2 + \text{I}^-(\text{H}_2\text{O})$. The results of previous restricted closed-shell B97-1/ECP/d simulations⁵⁴ (the same method used here) were used to determine the branching between the $[\text{CH}_3-\text{I}-\text{OH}]^-$ dissociation pathways. With ZPE included, the dissociation threshold for this complex is 50.7 kcal/mol. When the trajectories were terminated, the total energy of $[\text{CH}_3-\text{I}-\text{OH}]^-$ was always less than 70 kcal/mol.

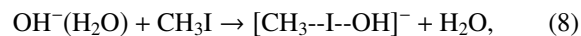


IV. COMPUTATIONAL REACTION DYNAMICS

The $\text{OH}^-(\text{H}_2\text{O}) + \text{CH}_3\text{I}$ reaction dynamics, versus collision impact parameter b , were studied at reactant relative collision energies E_{rel} of 0.05, 0.5, 1.0, and 2.0 eV. Reactant temperatures were chosen to match experiment^{17–19} as described above. For the four E_{rel} , in increasing order, a total of 736, 749, 766, and 894 trajectories were calculated.

A. Reaction probabilities versus impact parameter and reaction cross sections for different E_{rel}

Trajectories were calculated for b of 0, 1, 2, 3, 4, 4.5, and 5 Å at $E_{\text{rel}} = 2.0$ eV; 0, 1, 2, 3, 4, 5, 6, and 7 Å for $E_{\text{rel}} = 1.0$ eV; 0, 2, 4, 6, 7, and 8 Å for $E_{\text{rel}} = 0.5$ eV; and 0, 2, 4, 6, 8, 10, and 11 Å for $E_{\text{rel}} = 0.05$ eV. There were no reactions out of 100 trajectories at the largest b for each E_{rel} . Eleven product pathways were observed at the conclusion of the trajectories, of which eight involved formation of the complexes discussed above. However, from analyses of the energies of these complexes and their possible dissociation, as described in Sec. III, the following seven product channels were identified:



Reaction (9) has an extremely low probability, which is negligible compared to the other reactions. Reaction (11) is CID of the reactant $\text{OH}^-(\text{H}_2\text{O})$ and is not considered a product pathway.

Figure 4 plots, at different E_{rel} , the probability versus impact parameter $P_r(b)$ for reactions (5)–(8) and the total reaction probability. Overall, the total reaction probability increases as E_{rel} decreases. Identifying b_{max} as the largest impact parameter for which reaction occurred out of 100 trajectories, b_{max} increases as E_{rel} decreases. For E_{rel} of 2.0, 1.0, 0.5, and 0.05 eV, the value of b_{max} is 4.5, 6.0, 7.0, and 10.0 Å,

FIG. 4. Simulation probabilities, versus impact parameter, of five reaction pathways and total reaction: black circle with dotted line, total reaction; red diamond with dashed line, $\text{CH}_3\text{OH} + \text{I}^- + \text{H}_2\text{O}$ pathway; green triangle with dashed line, $\text{CH}_2\text{I}^- + 2\text{H}_2\text{O}$ pathway; pink square with solid line, $\text{CH}_3\text{OH} + \text{I}^-(\text{H}_2\text{O})$ pathway; blue square with dashed line, $[\text{CH}_3-\text{I}-\text{OH}]^- + \text{H}_2\text{O}$ pathway; orange dot with solid line, $\text{CH}_2\text{I}^-(\text{H}_2\text{O}) + \text{H}_2\text{O}$ pathway.

respectively. The increase in both the total reaction probability and b_{max} with decreasing E_{rel} is understood by recognizing that a lower E_{rel} allows longer interaction times and longer-range interactions between the two reactants.

The total reaction cross section σ_r was obtained by integrating the total reaction probability $P_r(b)$ over the impact parameter according to $\int P_r(b)2\pi b db$. The resulting cross section increases with decrease in collision energy and is 4.9 ± 0.5 , 13.3 ± 1.0 , 35.6 ± 2.0 , and $147.3 \pm 4.6 \text{ \AA}^2$ for E_{rel} of 2.0, 1.0, 0.5, and 0.05 eV, respectively. The cross sections for the individual reaction pathways were calculated in the same manner and are listed in Table II along with the total cross section. As shown in Table I, the CID channel is energetically feasible at E_{rel} of 2.0 eV and at this energy the simulations give a CID cross section of $9.1 \pm 0.9 \text{ \AA}^2$, which is larger than the reactive cross section of $4.9 \pm 0.5 \text{ \AA}^2$.

Among the four product pathways, the non-solvated-S_N2 pathway (reaction (5)) is most important. The probability of this pathway increases as E_{rel} decreases and it dominates at all E_{rel} , giving rise to the same increasing trend as the total reaction probability with decrease in E_{rel} . The solvated S_N2 pathway (reaction (6)) has a very low and similar probability for all E_{rel} . The proton transfer pathway (reaction (7)) is the second most important pathway at high E_{rel} , but is highly suppressed at low E_{rel} contributing only ~2% and 1% of the total reaction at 0.5 and 0.05 eV, respectively. On the contrary, the pathway forming [CH₃--I--OH]⁻ (reaction (8)) has a very low probability at low E_{rel} and high probability at high E_{rel} . The pathway forming CH₂I⁻(H₂O) (reaction (10)) has a similar yield for all E_{rel} , ranging from 2% to 6%.

As shown in Table I, proton transfer (reaction (7)) has an endothermicity of 23.6 kcal/mol with ZPE in the reactants and products. The small cross sections found for proton transfer at 0.5 and 0.05 eV (Table II), energies much below this endothermic barrier, result from the unphysical use of ZPE to promote reaction;⁵⁵ i.e., for each trajectory the products are formed without ZPE. For proton transfer forming CH₂I⁻(H₂O), reaction (10), the reaction endothermicity with ZPE included is 5.7 kcal/mol. Thus, the cross section observed for this reaction at 0.05 eV (1.2 kcal/mol) also results from the unphysical

use of ZPE. Dynamics associated with this unphysical use of ZPE to promote these endothermic reactions are considered in Sec. IV.

B. S_N2 atomistic dynamics

1. Mechanisms

Reactions (5), (6), and (9) are S_N2 reactions, and their atomic-level mechanisms were determined by animating the S_N2 trajectories. Both direct and indirect mechanisms were observed for all E_{rel} . Animations of representative trajectories for different mechanisms can be found at <http://hase-group.ttu.edu/group/animations/jingr2.html>.

Following previous studies for the OH⁻ + CH₃I S_N2 reaction,^{17,24,25} two types of direct mechanisms, called rebound and stripping, were identified for the OH⁻(H₂O) + CH₃I S_N2 reactions. For direct rebound (DR), OH⁻(H₂O) attacks the backside of CH₃I, directly displacing the I atom and scattering in the backward direction, with CH₃ inversion. For direct stripping (DS), OH⁻(H₂O) approaches the side of CH₃I, stripping off CH₃ and scattering in the forward direction, with CH₃ inversion.

Nine different indirect mechanisms were identified for the OH⁻(H₂O) + CH₃I S_N2 reaction. They are: (1) round-about (RA); (2) HO⁻--HCH₂I hydrogen-bonded pre-reaction complex (R1pre); (3) CH₃OH---I⁻ hydrogen-bonded post-reaction complex (R1post); (4) proton exchange between the HO⁻--HCH₂I and HOH---CH₂I⁻ complexes, (R1PE); (5) (H₂O)HO⁻--HCH₂I pre-reaction complex (R2pre); (6) (H₂O)CH₃OH---I⁻ post-reaction complex (R2post); (7) proton exchange between the (H₂O)HO⁻--HCH₂I and CH₂I⁻--H₂O(H₂O) complexes, (R2PE); (8) formation of the [CH₃--I--OH]⁻ complex, (C1); and (9) formation of the [CH₃--I--OH]⁻(H₂O) complex, (C2). There are 19 types of combined indirect mechanisms, which couple either 2 or 3 types of the above 9 indirect mechanism types: i.e., (10) RA + R1post, (11) RA + R2pre, (12) RA + R2PE, (13) RA + R1pre + R2pre, (14) RA + R2pre + R2PE, (15) RA + R2pre + C2, (16) R1pre + R1post, (17) R1pre + R1PE, (18) R1pre + R2pre, (19)

TABLE II. Cross sections versus E_{rel} for the different reaction pathways.^a

Pathway	E_{rel}			
	2.0	1.0	0.5	0.05
CH ₃ I + OH ⁻ + H ₂ O ^b	9.1 ± 0.6	2.0 ± 0.4	0.7 ± 0.3	1.3 ± 0.6
CH ₃ OH + I ⁻ + H ₂ O	2.8 ± 0.4	8.0 ± 0.9	26.1 ± 1.9	118.9 ± 4.8
CH ₃ OH + I ⁻ (H ₂ O)	0.1 ± 0.1	0.2 ± 0.1	1.0 ± 0.3	2.3 ± 0.7
CH ₂ I ⁻ + 2H ₂ O ^c	1.7 ± 0.3	2.7 ± 0.4	0.6 ± 0.3	0.8 ± 0.4
[CH ₃ --I--OH] ⁻ + H ₂ O	0.2 ± 0.1	2.1 ± 0.4	5.7 ± 0.9	21.8 ± 2.2
CH ₂ I ⁻ (H ₂ O) + H ₂ O ^d	0.1 ± 0.1	0.3 ± 0.2	2.2 ± 0.6	3.5 ± 1.0
Total reactive ^e	4.9 ± 0.5	13.3 ± 1.0	35.6 ± 2.0	147.3 ± 4.6

^a E_{rel} is in eV and cross section is in \AA^2 .

^bThis CID pathway is energetically closed at E_{rel} of 1.0 eV, and the dissociations observed in the trajectories at this E_{rel} and lower result from the incorrect use of reactant ZPE to promote dissociation.

^cThis pathway is energetically closed at E_{rel} of 0.5 and 0.05 eV, and the reaction observed in the trajectories at these E_{rel} result from the incorrect use of reactant ZPE to promote reaction. ZPE is also used to incorrectly enhance reaction at 1.0 eV.

^dThis pathway is energetically closed at E_{rel} of 0.05 eV, and the reaction observed in the trajectories at this E_{rel} results from the incorrect use of reactant ZPE to promote reaction.

^eThe total reactive cross section does not include the collision-induced dissociation pathway forming CH₃I + OH⁻ + H₂O.

R2pre + R1post, (20) R2pre + R1PE, (21) R2pre + R2post, (22) R2pre + R2PE, (23) R2-pre + C2, (24) R2pre + R2PE + R1post, (25) R1PE + R1post, (26) R2PE + R2post, (27) C2 + R2PE, and (28) C1 + C2.

For the RA mechanism,^{24,56} OH⁻(H₂O) collides with CH₃I and the CH₃-group rotates around I one or more times before S_N2 substitution. The roundabout mechanism occurs at the very early stage of the reaction and easily couples with other indirect mechanisms involving complex formation. There are 6 combined indirect mechanisms involving the roundabout mechanism; i.e., types 10–15.

For the R1pre, R1post, and R1PE indirect mechanisms, the H₂O molecule departs from CH₃I(OH⁻) during the OH⁻(H₂O) and CH₃I collision, and at an early stage of the trajectory. Then, for R1pre the HO⁻---HCH₂I hydrogen-bonded pre-reaction complex is formed, for R1post the CH₃OH---I⁻ hydrogen-bonded post-reaction complex is formed, and for R1PE the proton exchange HO⁻---HCH₂I and HOH---CH₂I⁻ complexes are formed. These three mechanisms tend to be high collision energy events. On the contrary, the indirect mechanisms R2pre, R2post, and R2PE, in which H₂O remains attached to CH₃I(OH⁻) during the reaction, tend to be low collision energy events. Proton-exchange-rotation,^{24,25} where the dehydrogenated CH₂-part rotates around the I atom and receives H back after one rotation, occurs for some of the trajectories. Although both the post-reaction CH₃OH---I⁻ and (H₂O)CH₃OH---I⁻ complexes are formed, they are less important than their corresponding pre-reaction complexes HO⁻---HCH₂I and (H₂O)HO⁻---HCH₂I.

Detailed dynamics of the H₂O molecule, for the different atomistic mechanisms, are discussed below in Sec. V C.

2. Probabilities of the atomistic mechanisms

As shown in Table III, the direct rebound mechanism tends to be a small impact parameter event, while direct stripping tends to occur at larger impact parameters. In contrast, the indirect mechanisms contribute at all impact parameters, except for the highest E_{rel} of 2.0 eV.

Cross sections were calculated for the different atomic-level mechanisms for the combined S_N2 pathways forming CH₃OH + I⁻ + H₂O or CH₃OH + I⁻(H₂O). The respective cross sections for the direct rebound, direct stripping, and indirect S_N2 mechanisms are 1.1 ± 0.3, 0.6 ± 0.2, and 1.2 ± 0.2; 2.1 ± 0.4, 2.0 ± 0.5, and 4.1 ± 0.7; 2.1 ± 0.5, 3.5 ± 0.8, and 21.5 ± 1.7; 13.0 ± 1.6, 16.6 ± 2.5, and 91.6 ± 4.6 Å² for 2.0, 1.0, 0.5, and 0.05 eV, respectively. The fractions between the direct and indirect mechanisms are 0.58:0.42; 0.50:0.50, 0.20:0.80, and 0.25:0.75 for 2.0, 1.0, 0.5, and 0.05 eV, respectively. At the high collision energies, the direct mechanisms are slightly more important than the indirect mechanisms, but at the low collision energies the indirect mechanisms dominate.

Fractions of the different atomistic mechanisms are summarized in Figure 5 for the four collision energies. To simplify the analyses, the 28 different mechanisms are grouped into 8 categories, for which 4 individual mechanisms are kept, i.e., DR, DS, HO⁻---HCH₂I hydrogen-bonded pre-reaction complex (R1pre), (H₂O)HO⁻---HCH₂I pre-reaction complex (R2pre). The remaining mechanisms are grouped into three

TABLE III. Percentages of different atomic-level mechanisms versus impact parameter for the OH⁻(H₂O) + CH₃I S_N2 reaction.

b^b	Direct ^a		
	DR	DS	Indirect
$E_{rel} = 2.0 \text{ eV}$			
0	30	0	70
1	33	0	67
2	44	11	44
3	33	0	67
4	33	67	0
4.5	0	100	0
$E_{rel} = 1.0 \text{ eV}$			
0	15	0	85
1	31	0	69
2	38	0	62
3	43	29	29
4	25	25	50
5	50	25	25
6	0	33	67
$E_{rel} = 0.5 \text{ eV}$			
0	15	0	85
2	7	2	91
4	12	8	80
6	0	29	71
7	0	44	56
$E_{rel} = 0.05 \text{ eV}$			
0	25	0	75
2	28	0	72
4	23	4	73
6	4	19	77
8	0	23	77
10	0	0	100

^aDR and DS are direct rebound and direct stripping, respectively.

^bThe impact parameter b is in unit of Å.

categories: i.e., mechanism with only R1PE and/or R2PE involved (PE), roundabout-involved mechanisms (*cRA*), [CH₃--I--OH]⁻ and [CH₃--I--OH]⁻(H₂O)-involved mechanisms (C1C2), and mechanisms where R1pre, R1post, R1PE, R2pre, R2post, and R2PE are combined (R1R2).

For some of the R2PE trajectories, in which the (H₂O)HO⁻---HCH₂I and CH₂I⁻---H₂O(H₂O) complexes are formed, the CH₃-group of the CH₃OH S_N2 product contains a H atom from the OH⁻(H₂O) reactant. The fraction of such trajectories is 0.0% for 2.0 eV, 1.0% for 1.0 eV, 4.5% for 0.5 eV, and 2.4% for 0.05 eV. If the isotopically substituted reaction OH⁻(H₂O) + CD₃I is studied, the products may be either CD₂HOH + I⁻ + HOD or CD₃OH + I⁻ + H₂O and this mechanism may be identified.

The relative importance of the different atomistic mechanisms depends on the collision energy. At 2.0 eV, direct rebound is the most important mechanism and of the indirect mechanisms, the roundabout is most important. Direct rebound remains the most important at 1.0 eV, but proton exchange (i.e., HO⁻---HCH₂I ↔ HOH---CH₂I⁻) with and without the H₂O molecule becomes the most important indirect mechanism. At the low collision energies of 0.5 and 0.05 eV, the indirect mechanisms become much

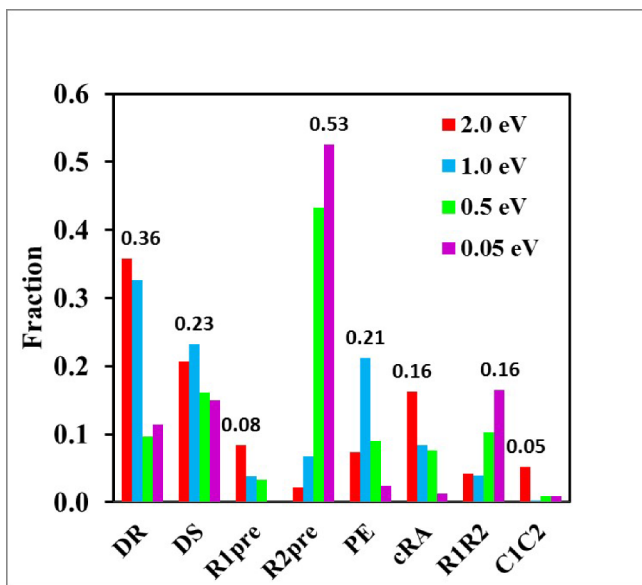


FIG. 5. Fractions of the atomic reaction mechanisms for the $\text{OH}^-(\text{H}_2\text{O}) + \text{CH}_3\text{I} \rightarrow \text{CH}_3\text{OH} + \text{I}^- + \text{H}_2\text{O}$ and $\text{OH}^-(\text{H}_2\text{O}) + \text{CH}_3\text{I} \rightarrow \text{CH}_3\text{OH} + \text{I}^-(\text{H}_2\text{O})$ $\text{S}_{\text{N}}2$ reactions, at the different E_{rel} : DR, direct rebound; DS, direct stripping; R1pre, $\text{HO}^-\text{---HCH}_2\text{I}$ complex formation; R2pre, $(\text{H}_2\text{O})\text{HO}^-\text{---HCH}_2\text{I}$ complex formation; R2PE, proton exchange; cRA, roundabout involved; R1R2, combination mechanisms of R1pre, R2pre, R1post, R2post, R1PE, and R2PE; C1C2, $[\text{CH}_3\text{---I---OH}]^-$ and $[\text{CH}_3\text{---I---OH}]^-(\text{H}_2\text{O})$ involved. The fractions are based on the cross sections. The highest value of each mechanism is labeled. For 2.0, 1.0, 0.5, and 0.05 eV, the respective fractions with errors are: DR mechanism, 0.36 ± 0.08 , 0.25 ± 0.11 , 0.07 ± 0.04 , and 0.10 ± 0.02 ; DS mechanism, 0.21 ± 0.14 , 0.23 ± 0.16 , 0.12 ± 0.06 , and 0.13 ± 0.04 ; and R2pre mechanism, 0.02 ± 0.02 , 0.07 ± 0.04 , 0.44 ± 0.09 , and 0.53 ± 0.08 .

more important and the mechanism with formation of the $(\text{H}_2\text{O})\text{HO}^-\text{---HCH}_2\text{I}$ pre-reaction complex dominates.

3. $\text{I}^-(\text{H}_2\text{O})$ formation

It is of particular interest to identify the mechanisms for solvation of I^- to form $\text{I}^-(\text{H}_2\text{O})$. At E_{rel} of 2.0 eV, only one trajectory forms $\text{I}^-(\text{H}_2\text{O})$ and it is a direct rebound event. At 1.0 eV, six trajectories form $\text{I}^-(\text{H}_2\text{O})$, with half direct rebound and half indirect. For E_{rel} of 0.5 and 0.05 eV, the yields of $\text{I}^-(\text{H}_2\text{O})$ are higher and the statistics are better for the analyses. Approximately 80% and 90% of the reaction is indirect at 0.5 and 0.05 eV, respectively. The important indirect mechanisms are $(\text{H}_2\text{O})\text{HO}^-\text{---HCH}_2\text{I}$ pre-reaction complex formation and $(\text{H}_2\text{O})\text{HO}^-\text{---HCH}_2\text{I} \leftrightarrow \text{CH}_2\text{I}^-\text{---H}_2\text{O}(\text{H}_2\text{O})$ proton-exchange.

C. Proton transfer atomistic dynamics

Reactions (7) and (10) are proton transfer and their atomic-level mechanisms were also identified by animating the trajectories. As discussed in Sec. IV A, the proton transfer observed for reaction (7) at the low E_{rel} of 0.5 and 0.05 eV, and for reaction (10) at 0.05 eV is unphysical. Hence, only the proton transfer at E_{rel} of 1.0 and 2.0 eV for reaction (7) and 0.5, 1.0, and 2.0 eV for reaction (10) are discussed. Direct rebound, direct stripping, and indirect mechanisms were observed for both reactions (7) and (10). The first two mechanisms are quite similar to those for $\text{S}_{\text{N}}2$ reactions.

There are multiple indirect mechanisms for $\text{OH}^-(\text{H}_2\text{O}) + \text{CH}_3\text{I} \rightarrow \text{CH}_2\text{I}^- + 2\text{H}_2\text{O}$ proton transfer. They include the same types of mechanisms as for the $\text{S}_{\text{N}}2$ reaction: i.e., (1) RA, (2) R1pre, (4) R1PE, (5) R2pre, (7) R2PE, (8) C1, and (9) C2; and two new indirect mechanisms, i.e., (3) formation of the $\text{CH}_2\text{I}^-\text{---H}_2\text{O}$ post-reaction complex (R1pt) and (6) formation of the $\text{CH}_2\text{I}^-\text{---H}_2\text{O}(\text{H}_2\text{O})$ post-reaction complex (R2pt). In addition, there are 11 types of combined indirect mechanisms, including (10) RA + R1pre, (11) RA + R1pt, (12) RA + R1pre + R1pt, (13) RA + R2pre + R1pre + R1pt, (14) RA + $\text{S}_{\text{N}}2$ barrier-recrossing, (15) R1pre + R1pt, (16) R2pre + R1pt, (17) R2pre + R1pre + R1pt, (18) R2pre + R2pt + R1pre + R1pt, (19) R2pre + R2PE + R1pre + R1PE, and (20) R2pt + R1pt.

As for the $\text{S}_{\text{N}}2$ indirect mechanisms, the indirect mechanisms for reaction (7) proton transfer were grouped into the following three categories to determine mechanistic probabilities: i.e., roundabout-involved mechanisms (cRA), $[\text{CH}_3\text{---I---OH}]^-$ and $[\text{CH}_3\text{---I---OH}]^-(\text{H}_2\text{O})$ -involved mechanisms (C1C2), and mechanisms where R1pre, R1pt, R1PE, R2pre, R2pt, and R2PE are combined (R1R2). At 2.0 eV, 0.55 ± 0.018 of reaction (7) is direct, with DR = 0.28 ± 0.09 and DS = 0.27 ± 0.09 . The indirect mechanisms CRA, C1C2, and R1R2 contribute 0.25 ± 0.08 , 0.12 ± 0.04 , and 0.08 ± 0.03 , respectively. The importance of the roundabout-involved mechanisms at the high E_{rel} of 2.0 eV is the same as found for the $\text{S}_{\text{N}}2$ reaction.

Proton transfer forming $\text{CH}_2\text{I}^- + 2\text{H}_2\text{O}$, reaction (7), has an endothermicity including ZPE of 23.6 kcal/mol (Table I and Figure 2), which is slightly higher than the 1.0 eV (23.1 kcal/mol) collision energy. However, with the reactants' thermal vibrational and rotational energy included, the average energy of the reactants exceeds this endothermic threshold. Nevertheless, the reaction observed at $E_{\text{rel}} = 1.0$ eV is unphysical, since the total vibrational energy of $\text{CH}_2\text{I}^- + 2\text{H}_2\text{O}$ is less than the ZPE for each of the trajectories. As discussed below in Sec. V B, this results in a simulation cross section much larger than the experimental value. Dynamics associated with these unphysical trajectories are considered in Sec. VI.

The probability of $\text{CH}_2\text{I}^-(\text{H}_2\text{O})$ formation, reaction (10), increases with decrease in E_{rel} , which is expected since there is less energy available to dissociate H_2O from $\text{CH}_2\text{I}^-(\text{H}_2\text{O})$ as E_{rel} is lowered. At E_{rel} of 2.0 eV, only one trajectory formed $\text{CH}_2\text{I}^-(\text{H}_2\text{O})$ and its mechanism is direct rebound. At E_{rel} of 1.0 and 0.5 eV, the fraction of the reaction which is indirect is 0.26 ± 0.13 and 0.65 ± 0.26 , respectively.

Indirect mechanisms for reaction (10), $\text{CH}_2\text{I}^-(\text{H}_2\text{O}) + \text{H}_2\text{O}$ formation, have multiple features. Mechanisms for most indirect trajectories were roundabout, coupling between the $(\text{H}_2\text{O})\text{HO}^-\text{---HCH}_2\text{I}$ pre-reaction and $\text{CH}_2\text{I}^-\text{---H}_2\text{O}(\text{H}_2\text{O})$ post-reaction complexes, and coupling of the roundabout with one or both of these complexes. If H_2O dissociates from $\text{OH}^-(\text{H}_2\text{O})$ before proton transfer occurs, the water molecule attached to CH_2I^- contains a H-atom from CH_3I . In contrast, for some of the indirect trajectories, the free H_2O molecule contained a H-atom from CH_3I . The percentage of such trajectories, among all the $\text{CH}_2\text{I}^-(\text{H}_2\text{O}) + \text{H}_2\text{O}$ trajectories, is 2% for 1.0 eV and 42% for 0.5 eV. These dynamics occur when the post-reaction complex $\text{CH}_2\text{I}^-\text{---H}_2\text{O}(\text{H}_2\text{O})$

is formed and either of the two H_2O molecules may attach to CH_2I^- . For the direct rebound and stripping trajectories forming $\text{CH}_2\text{I}^-(\text{H}_2\text{O}) + \text{H}_2\text{O}$, the free water molecule never contains the H-atom from CH_3I . Identification of which H_2O molecule contains the H-atom from CH_3I may be determined experimentally by studying the isotopically substituted reaction $\text{OH}^-(\text{H}_2\text{O}) + \text{CD}_3\text{I}$, which can form either $\text{CD}_2\text{I}^-(\text{H}_2\text{O})$ or $\text{CD}_2\text{I}^-(\text{HOD})$.

As discussed in the previous study²⁵ and shown in Figure 3, the $\text{OH}^- + \text{CH}_3\text{I}$ $\text{S}_{\text{N}}2$ and proton transfer reactions share the same pre-reaction complex $\text{HO}^- - \text{HCH}_2\text{I}$. Differences in their atomistic mechanisms involve formation of different post-reaction complexes, i.e., $\text{CH}_3\text{OH} - \text{I}^-$ for the $\text{S}_{\text{N}}2$ reaction and $\text{CH}_2\text{I}^- - \text{H}_2\text{O}$ for proton transfer.

D. Product distributions for the $\text{S}_{\text{N}}2$ reaction

1. Internal energy

The distribution of the product pseudo internal energy $p\text{-}E_{\text{int}}$ (see Sec. II B) for the $\text{OH}^-(\text{H}_2\text{O}) + \text{CH}_3\text{I} \rightarrow \text{CH}_3\text{OH} + \text{I}^- + \text{H}_2\text{O}$ $\text{S}_{\text{N}}2$ reaction is plotted in Figure 6 for the different E_{rel} . The average fraction of the available product energy partitioned to E_{int} , i.e., f_{int} , is 0.79 ± 0.20 , 0.80 ± 0.19 , 0.84 ± 0.10 , and 0.85 ± 0.08 at E_{rel} of 2.0, 1.0, 0.5, and 0.05 eV, respectively. The value for f_{int} depends upon the reaction mechanism, and f_{int} for the direct rebound, direct stripping, and indirect mechanisms are compared in Table IV. At the higher E_{rel} of 2.0 eV, the indirect mechanisms partition more energy to the product internal degrees of freedom, while for the lowest E_{rel} of 0.05 eV the energy partitioning is similar for the three mechanisms.

2. Velocity scattering angle

Velocity scattering angle distributions, between the velocity vectors of CH_3I and I^- are given in Figure 7 for the

$\text{OH}^-(\text{H}_2\text{O}) + \text{CH}_3\text{I} \rightarrow \text{CH}_3\text{OH} + \text{I}^- + \text{H}_2\text{O}$ $\text{S}_{\text{N}}2$ reaction's direct rebound, direct stripping, and indirect mechanisms. For $\cos \theta$ less than zero, the scattering is backward with I^- scattering back in the opposite direction of the CH_3I initial velocity vector. For forward scattering, $\cos \theta$ is greater than zero. The scattering distributions for these mechanisms are different and similar, respectively, to those determined from previous B97-1/ECP/d simulations for $\text{F}^- + \text{CH}_3\text{I}$ and $\text{OH}^- + \text{CH}_3\text{I}$ $\text{S}_{\text{N}}2$ reactions.²⁴ Rebound and stripping are “overall” backward and forward scattering events, respectively, while the scattering for the indirect mechanisms is quite isotropic. As shown in Figure 8, combination of the scattering for these three mechanisms gives a total scattering angle distribution which is approximately isotropic for each collision energy.

The $\text{S}_{\text{N}}2$ mechanisms, i.e., rebound, stripping, and indirect, were identified by animating the trajectories. As shown in Figure 7, some of the rebound events have $\cos \theta$ greater than zero, as a result of the formation of the three reaction products $\text{CH}_3\text{OH} + \text{I}^- + \text{H}_2\text{O}$. Calculating the scattering angle between CH_3I and I^- , and not between CH_3I and unbound $\text{I}^- - \text{H}_2\text{O}$, may result in $\cos \theta$ greater than zero.

3. $\text{I}^-(\text{H}_2\text{O})$

As discussed above (Sec. IV B 3 and Table II), the yield of $\text{I}^-(\text{H}_2\text{O})$ is quite small and there are insufficient number of trajectory events forming this product to determine distributions for its internal energy and velocity scattering angle. However, averages may be determined for these properties. The average fraction f_{int} of the available product energy partitioned to $\text{CH}_3\text{OH} + \text{I}^-(\text{H}_2\text{O})$ pseudo-internal energies, $p\text{-}E_{\text{int}}$ (Sec. II B), is 0.87 ± 0.43 , 0.96 ± 0.36 , and 0.98 ± 0.39 at E_{rel} of 1.0, 0.5, and 0.05 eV, respectively. These fractions are similar to those in Table IV for $\text{CH}_3\text{OH} + \text{I}^- + \text{H}_2\text{O}$ formed by the indirect mechanisms. For E_{rel} of 0.5 and 0.05 eV, there are a sufficient number of trajectory events to consider the nature

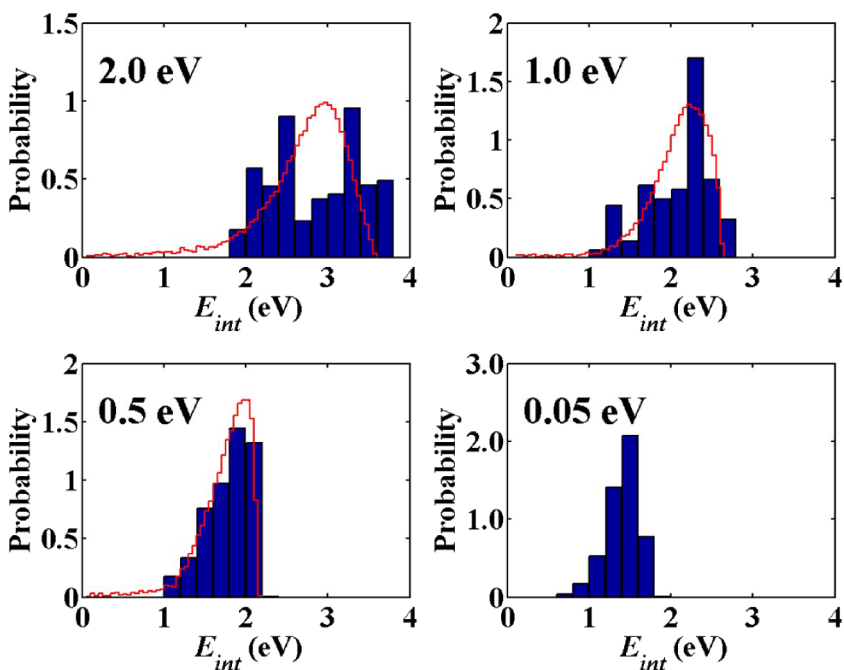


FIG. 6. Simulation (black histogram) and experiment (red curve) product pseudo internal energy distributions for the $\text{OH}^-(\text{H}_2\text{O}) + \text{CH}_3\text{I} \rightarrow \text{CH}_3\text{OH} + \text{I}^- + \text{H}_2\text{O}$ $\text{S}_{\text{N}}2$ reaction at the different E_{rel} . The probability is the fraction of trajectories within the bar width, divided by the bar width. The total area under each curve and histogram is unity.

TABLE IV. Fractions of the available product energy partitioned to internal energy for $\text{OH}^-(\text{H}_2\text{O}) + \text{CH}_3\text{I} \rightarrow \text{CH}_3\text{OH} + \text{I}^- + \text{H}_2\text{O}$.^a

E_{rel} (eV)	Mechanism ^b			Total ^c	Expt. ^d
	DR	DS	Ind		
2.0	0.76 ± 0.11	0.64 ± 0.09	0.91 ± 0.13	0.79 ± 0.11	0.75
1.0	0.73 ± 0.08	0.70 ± 0.08	0.91 ± 0.10	0.80 ± 0.09	0.80
0.5	0.73 ± 0.03	0.73 ± 0.03	0.87 ± 0.06	0.84 ± 0.06	0.82
0.05	0.80 ± 0.03	0.76 ± 0.03	0.86 ± 0.03	0.85 ± 0.03	

^aThe partitioning is to pseudo internal energy; see Sec. II B.

^bDR, DS, and Ind are the direct rebound, direct stripping, and indirect mechanisms.

^cThe result for the combined DR, DS, and Ind mechanisms.

^dThe experimental results, Ref. 27.

of velocity scattering angle distribution. For both energies it appears to be isotropic, with statistically the same amount of forward and backward scattering, with respective average $\cos \theta$ values of 0.01 ± 0.37 and 0.12 ± 0.40 .

V. DISCUSSION

A. Comparison with simulations of the $\text{OH}^- + \text{CH}_3\text{I}$ reaction dynamics

It is of interest to compare the reaction mechanisms, and their probabilities and cross sections, determined from simulations for OH^- and $\text{OH}^-(\text{H}_2\text{O})$ reacting with CH_3I . If the collision-induced dissociation channel $\text{OH}^-(\text{H}_2\text{O}) + \text{CH}_3\text{I} \rightarrow \text{OH}^- + \text{H}_2\text{O} + \text{CH}_3\text{I}$ is not included, the total reaction cross section for $\text{OH}^-(\text{H}_2\text{O})$ is smaller than that for OH^- at E_{rel} of 2.0, 1.0, and 0.5 eV, but statistically the same as that for OH^- at the lowest E_{rel} of 0.05 eV, i.e., $132.5 \pm 10.3 \text{ \AA}^2$ for OH^- and $147.3 \pm 4.6 \text{ \AA}^2$ for $\text{OH}^-(\text{H}_2\text{O})$. Their difference is greatest at 2.0 eV, where the respective OH^- and $\text{OH}^-(\text{H}_2\text{O})$ total reaction cross sections are 14.0 ± 1.9 and $4.9 \pm 0.5 \text{ \AA}^2$. The total reaction rate constant is ~ 2 times larger for OH^- ; see Figure 9.

The S_N2 reaction forming $\text{CH}_3\text{OH} + \text{I}^-$ is the most important pathway for OH^- and the S_N2 reaction forming $\text{CH}_3\text{OH} + \text{I}^- + \text{H}_2\text{O}$ is most important for $\text{OH}^-(\text{H}_2\text{O})$. For $\text{OH}^-(\text{H}_2\text{O})$, the $\text{CH}_3\text{OH} + \text{I}^-(\text{H}_2\text{O})$ products make a small and insignificant contribution to the S_N2 reaction. For OH^- , the cross section for proton transfer to form $\text{CH}_2\text{I}^- + \text{H}_2\text{O}$ is larger than the cross section for the S_N2 reaction at E_{rel} of 2.0, 1.0, and 0.5 eV. The S_N2 cross section becomes large at 0.05 eV. For the S_N2 pathway and at E_{rel} of 2.0 eV, the cross section for OH^- is $4.3 \pm 1.0 \text{ \AA}^2$ and statistically the same as that of $2.9 \pm 0.4 \text{ \AA}^2$ for $\text{OH}^-(\text{H}_2\text{O})$. For the lowest E_{rel} of 0.05 eV, the $\text{OH}^-(\text{H}_2\text{O})$ cross section for the S_N2 pathway is $118.9 \pm 4.8 \text{ \AA}^2$ and somewhat larger than the OH^- value of $76.0 \pm 9.7 \text{ \AA}^2$. For $\text{OH}^-(\text{H}_2\text{O})$, the dissociating H_2O molecule may “carry away” a sufficient amount of energy to form a stable $[\text{CH}_3-\text{I}-\text{OH}]^-$ ion, which contributes $\sim 15\%$ of the reaction at both 0.5 and 0.05 eV. It is the second most important pathway at these energies.

Proton transfer is significantly suppressed for $\text{OH}^-(\text{H}_2\text{O})$; i.e., the cross section for OH^- is ~ 6 times larger than that for $\text{OH}^-(\text{H}_2\text{O})$ at E_{rel} of 2.0 eV, and proton transfer is energetically closed for $\text{OH}^-(\text{H}_2\text{O})$ at 0.5 and 0.05 eV. As discussed above (Sec. IV C) and below (Sec. V B), the large cross section found

for $\text{OH}^-(\text{H}_2\text{O})$ proton transfer at 1.0 eV is incorrect as a result of forming products without ZPE. An important component in suppressing proton transfer for $\text{OH}^-(\text{H}_2\text{O})$ is the endothermicity of the pathways with a water molecule attached, as compared to the exothermic reactions for bare OH^- .

The S_N2 mechanisms are direct rebound, direct stripping, and indirect, for both OH^- and $\text{OH}^-(\text{H}_2\text{O})$, but their contributions are different for these two reactants. For the high E_{rel} of 2.0 and 1.0 eV, the direct and indirect mechanisms have similar probabilities for $\text{OH}^-(\text{H}_2\text{O})$, but the indirect mechanism contributes little (i.e., 5% at 2.0 eV and 20% at 1.0 eV) for OH^- . At the lower E_{rel} of 0.5 and 0.05 eV, the indirect mechanism contributes $\sim 40\%$ of the reaction for OH^- but, as shown in Table III and Figure 5, dominates the reaction for $\text{OH}^-(\text{H}_2\text{O})$. Thus, adding a H_2O molecule to OH^- increases the probability of the indirect mechanisms. Also, adding a H_2O molecule to the reactant substantially increases the number of the atomic-level indirect mechanisms. For $\text{OH}^- + \text{CH}_3\text{I}$ there are only seven atomistic indirect mechanisms, but as discussed above in Sec. IV B 1, there are 28 for $\text{OH}^-(\text{H}_2\text{O})$. The sum of the probabilities of the indirect mechanisms for the OH^- and $\text{OH}^-(\text{H}_2\text{O})$ S_N2 reactions versus E_{rel} of 0.05, 0.5, 1.0, and 2.0 eV are, respectively, 0.39 ± 0.07 , 0.42 ± 0.14 , 0.19 ± 0.13 , and 0.04 ± 0.02 for OH^- and 0.76 ± 0.09 , 0.80 ± 0.10 , 0.52 ± 0.17 , and 0.44 ± 0.15 for $\text{OH}^-(\text{H}_2\text{O})$. The addition of the H_2O molecule clearly increases the complexity of the PES for the $\text{OH}^-(\text{H}_2\text{O})$ reactant, resulting in more stationary points and product channels, but the manner in which this affects the S_N2 atomistic mechanisms is not clear.

The relative importance of the direct rebound and stripping mechanisms is different for the OH^- and $\text{OH}^-(\text{H}_2\text{O})$ S_N2 reactions. For OH^- , stripping is much more important than rebound for E_{rel} of 2.0, 1.0, and 0.5 eV, while the rebound and stripping probabilities are similar at 0.05 eV. This preference for stripping gives rise to velocity scattering angle distributions with enhanced probabilities for forward scattering at E_{rel} of 2.0, 1.0, and 0.5 eV for $\text{OH}^- + \text{CH}_3\text{I} \rightarrow \text{CH}_3\text{OH} + \text{I}^-$. For E_{rel} of 0.05 eV, the scattering is nearly isotropic.

For the $\text{OH}^-(\text{H}_2\text{O})$, S_N2 reaction rebound is somewhat more important than stripping at E_{rel} of 2.0 and 1.0 eV, while stripping is more important than rebound at the lower E_{rel} of 0.5 and 0.05 eV. The combination of the scattering angles for the direct rebound, direct stripping, and indirect mechanisms gives a nearly isotropic velocity scattering angle distribution at each E_{rel} for the $\text{OH}^-(\text{H}_2\text{O}) + \text{CH}_3\text{I}$ S_N2 reaction.

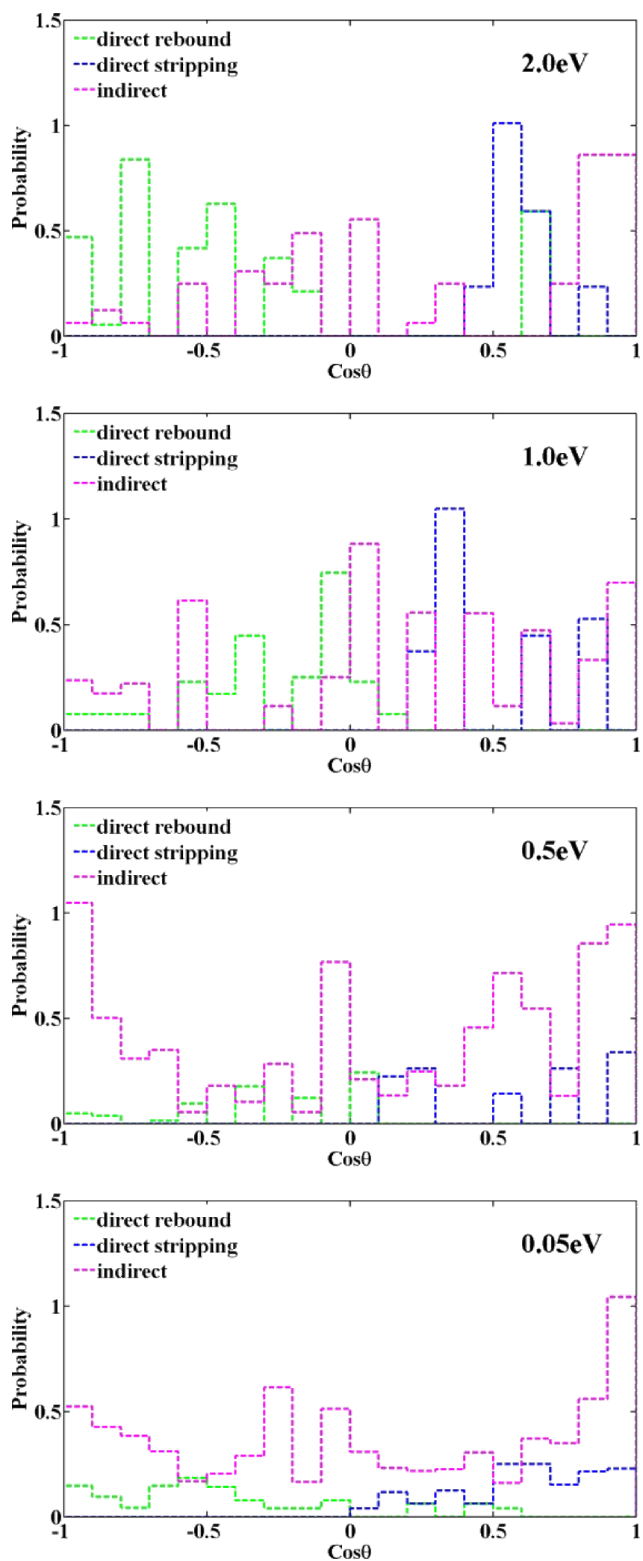


FIG. 7. Simulation distribution of velocity scattering angles for different atomistic mechanisms of the $\text{OH}^-(\text{H}_2\text{O}) + \text{CH}_3\text{I} \rightarrow \text{CH}_3\text{OH} + \text{I}^- + \text{H}_2\text{O}$ S_N2 reaction at different E_{rel} . Distributions are given for the direct rebound (green), direct stripping (blue), and indirect (pink) atomic-level mechanisms. The probability is the fraction of trajectories within the bar width, divided by the bar width. The total area under each histogram is unity.

Otto and Wester²⁷ have suggested that the presence of the linear-like $\text{HO}^- \cdots \text{CH}_3\text{I}$ pre-reaction complex for $\text{OH}^-(\text{H}_2\text{O})$, but not for OH^- , may enhance the rebound mechanism for $\text{HO}^-(\text{H}_2\text{O})$ as compared to OH^- , explaining the simulation

results. However, the influence of this complex at the high 2.0 eV collision energy is somewhat uncertain.

B. Comparison with experiment

In the following, properties of the $\text{OH}^-(\text{H}_2\text{O}) + \text{CH}_3\text{I}$ reaction, obtained from the simulations, are compared with experiment.^{17–19,23,27,57} These properties include the branching ratio between the different product anions, the reaction rate constant and CID cross section, and distributions of the velocity scattering angle and internal energy of the S_N2 products, including those for the $\text{CH}_3\text{OH} + \text{I}^-(\text{H}_2\text{O})$ pathway, and probabilities for forming the proton transfer products CH_2I^- and $\text{CH}_2\text{I}^-(\text{H}_2\text{O})$.

Branching between the I^- , CH_2I^- , $[\text{CH}_3-\text{I}-\text{OH}]^-$, and $\text{I}^-(\text{H}_2\text{O})$ product ions, found from the simulations and experiments, is compared in Table V. Overall, there is quite good agreement. For both, I^- is most and $\text{I}^-(\text{H}_2\text{O})$ least important. As shown in Figure 10, the relative yield of these two ions from the simulations and experiments is in excellent agreement. Ions detected with the mass of $[\text{CH}_3-\text{I}-\text{OH}]^-$ were identified as $\text{CH}_2\text{I}^-(\text{H}_2\text{O})$ in the experiments.^{17,27}

An ion with the mass of $[\text{CH}_3-\text{I}-\text{OH}]^-(\text{H}_2\text{O})$ was observed in the experiments, identified as $\text{I}^-(\text{CH}_3\text{OH})(\text{H}_2\text{O})$, and assumed to be formed by a third-body collision. In the simulations, $[\text{CH}_3-\text{I}-\text{OH}]^-(\text{H}_2\text{O})$ and $\text{I}^-(\text{CH}_3\text{OH})(\text{H}_2\text{O})$ are transient intermediates with sufficient energy to dissociate.

The major differences between the simulation and experiment ion yields are for the $[\text{CH}_3-\text{I}-\text{OH}]^-$ and CH_2I^- ions. At 0.5 eV, the simulations give significantly more $[\text{CH}_3-\text{I}-\text{OH}]^-$ than seen in the experiments. As discussed above in Sec. IV A, formation of CH_2I^- at E_{rel} of 0.5 and 0.05 eV is physically unrealistic, since the reaction endothermicity is higher than the reactants' energy. For each trajectory, the products are formed without ZPE. The average energy of the reactants, for the $E_{rel} = 1.0$ eV simulations, exceeds the proton transfer endothermicity of 23.6 kcal/mol and reaction is possible. However, the total vibrational energy of $\text{CH}_2\text{I}^- + 2\text{H}_2\text{O}$ is less than the ZPE for each of the trajectories, resulting in a cross section much larger than experiment. It is noteworthy that at the much higher E_{rel} of 2.0 eV, the CH_2I^- yield from the simulations is in approximate agreement with experiment.

The threshold energies of 1.1 eV and 0.4 eV deduced from the experiments for forming CH_2I^- and an ion with the mass of $\text{CH}_2\text{I}^-(\text{H}_2\text{O})/\text{CH}_3\text{I}(\text{OH}^-)$ are in good agreement with the electronic structure calculations reported in Table I. With ZPE included, the calculated threshold for forming CH_2I^- is 23.6 kcal/mol (1.0 eV). As discussed above, the product ion $\text{CH}_2\text{I}^-(\text{H}_2\text{O})$ is observed in the simulations, but $\text{CH}_3\text{I}(\text{OH}^-)$ is not. The calculated threshold for forming this latter ion is 7.6 kcal/mol (0.33 eV). The calculated threshold for forming $\text{CH}_2\text{I}^-(\text{H}_2\text{O})$ is 5.7 kcal/mol (0.25 eV).

The total rate constant for the $\text{OH}^-(\text{H}_2\text{O}) + \text{CH}_3\text{I}$ reaction has been measured⁵⁷ at $E_{rel} = 0.05$ eV and is $9.1 \pm 1.7 \times 10^{-10} \text{ cm}^3/\text{molecule s}$. The simulation total rate constant for this E_{rel} is $8.6 \pm 0.5 \times 10^{-10} \text{ cm}^3/\text{molecule s}$ and in excellent agreement with experiment. Similarly, the experimental and simulation total rate constants agree for the $\text{OH}^- + \text{CH}_3\text{I}$ reaction and the respective values are 1.90 ± 0.45 and

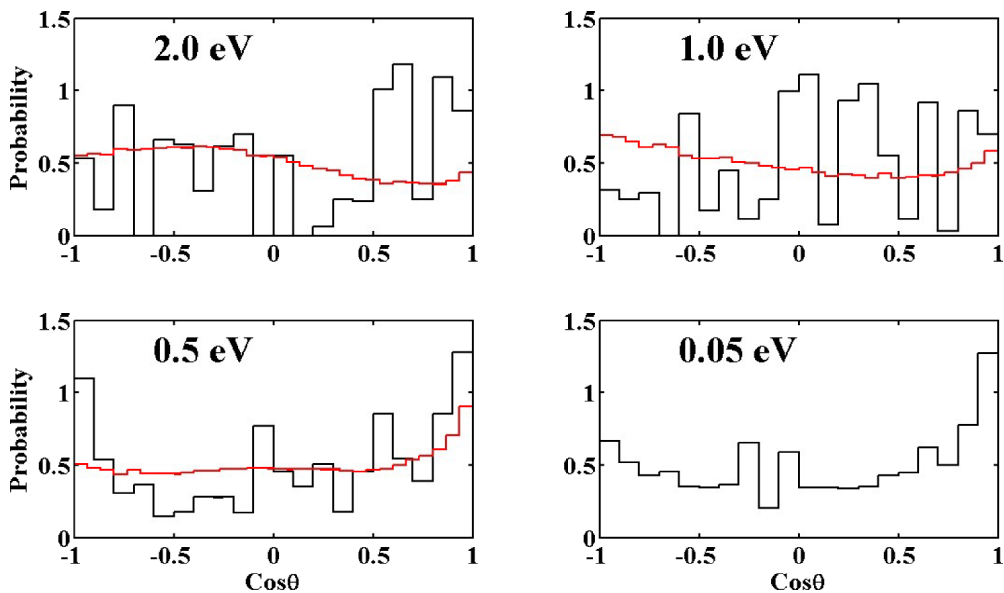


FIG. 8. Simulation (histogram) and experiment (curve) distributions of the total velocity scattering angles for the $\text{OH}^-(\text{H}_2\text{O}) + \text{CH}_3\text{I} \rightarrow \text{CH}_3\text{OH} + \text{I}^- + \text{H}_2\text{O}$ S_N2 reaction at different E_{rel} . The probability is the fraction of trajectories within the bar width, divided by the bar width. The total area under each curve and histogram is unity.

$2.03 \pm 0.16 \times 10^{-9} \text{ cm}^3/\text{molecule s}$. At 2.0 eV, the simulation cross section is $9.1 \pm 0.1 \text{ \AA}^2$ for forming the CID products $\text{OH}^- + \text{H}_2\text{O} + \text{CH}_3\text{I}$, which is similar to the respective experimental²³ CID cross sections of 12.1 and 12.8 \AA^2 for $\text{OH}^-(\text{H}_2\text{O}) + \text{CH}_3\text{Cl}$ and $\text{OH}^-(\text{H}_2\text{O}) + \text{CH}_3\text{Br}$, also at 2.0 eV. The somewhat higher cross sections for the experiments may arise from their higher 300 K temperature for $\text{OH}^-(\text{H}_2\text{O})$ as compared to 100 K for the simulations.

The simulation and experimental velocity scattering angle distributions, for the S_N2 $\text{CH}_3\text{OH} + \text{I}^- + \text{H}_2\text{O}$ products, are compared in Figure 7. Though the simulation and experiment distributions are not strikingly different, they are only in approximate agreement at E_{rel} of 1.0 and 0.5 eV. At 1.0 and 0.5 eV, 59% and 38% of the experimental scattering is in the backward direction, while these percentages from the

simulation are 48 ± 12 and 46 ± 5 . For the high E_{rel} of 2.0 eV, 81% of the scattering is in the backward direction for the experiments, while only $51\% \pm 14\%$ is backward for the simulation. There is substantial forward scattering in the simulations for $\cos \theta$ near unity. Since the rebound mechanism preferentially leads to backward scattering, the experiments indicate that the simulations underestimate the importance of the rebound mechanism at 2.0 eV. As shown in Figure 5, the rebound mechanism is most important at 2.0 eV for the simulations, but not of sufficient importance to give a backward scattering probability in agreement with experiment. In summary, in the simulations the probability of backward and forward scattering is statistically the same at each E_{rel} , while in the experiments the probability of backward scattering increases from 38% to 81% as E_{rel} is increased from 0.5 to 2.0 eV.

Though there are differences in the simulation and experiment velocity scattering angle distributions, the simulation and experiment product energy partitionings are similar. As shown in Figure 6, the experiment and simulation distributions of the pseudo internal energy $p\text{-}E_{int}$ of the $\text{CH}_3\text{OH} + \text{H}_2\text{O}$ products, for the $\text{OH}^-(\text{H}_2\text{O}) + \text{CH}_3\text{I} \rightarrow \text{CH}_3\text{OH} + \text{I}^- + \text{H}_2\text{O}$ S_N2 reaction, are in quite good agreement. At each E_{rel} , the average fraction f_{int} of the available energy partitioned to $p\text{-}E_{int}$ is statistically the same for the simulations and experiments; see Table IV.

The experimental and simulation scattering dynamics are also similar for the microsolvated S_N2 product ion $\text{I}^-(\text{H}_2\text{O})$. As shown in Figure 2 of Ref. 18 for the experiments, and described above in Sec. IV D 1 for the simulations, the product energy is preferentially partitioned to the pseudo internal energy of the $\text{CH}_3\text{OH} + \text{I}^-(\text{H}_2\text{O})$ products and the scattering is isotropic as expected for indirect and statistical dynamics. This scattering is similar to that observed in the experiments^{18,27} for $\text{CH}_3\text{OH} + \text{I}^- + \text{H}_2\text{O}$ products with large f_{int} and in the simulations for $\text{CH}_3\text{OH} + \text{I}^- + \text{H}_2\text{O}$ formed by the indirect mechanisms (Table IV).

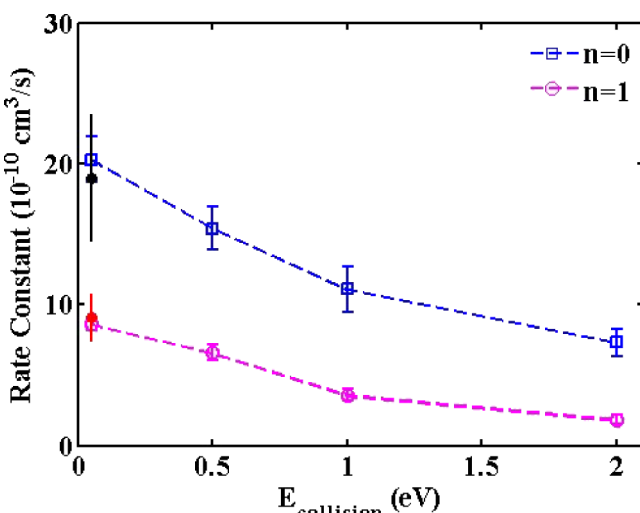


FIG. 9. Comparison of rate constant for CH_3I reacting with $\text{OH}^-(\text{H}_2\text{O})_{n=0,1}$, where n is the number of H_2O molecules, as a function of E_{rel} . Experiment values are solid points.

TABLE V. Comparison of experiment and simulation product anion ratios for the $\text{OH}^-(\text{H}_2\text{O}) + \text{CH}_3\text{I}$ reaction in gas phase.

E_{rel} (eV)		I^-	$\text{I}^-(\text{H}_2\text{O})$	CH_2I^- ^a	$[\text{CH}_3-\text{I}-\text{OH}]^-$ ^b	$\text{CH}_2\text{I}^-(\text{H}_2\text{O})$
2.0 (1.97) ^c	Simulation	0.57 ± 0.10	0.01 ± 0.01	0.35 ± 0.07	0.04 ± 0.02	0.03 ± 0.02
	Expt.	0.75	0.01	0.21	0.04	
1.0 (0.98)	Simulation	0.60 ± 0.08	0.02 ± 0.01	0.20 ± 0.04	0.16 ± 0.03	0.02 ± 0.02
	Expt.	0.92	0.01	0.02	0.05	
0.5 (0.48)	Simulation	0.73 ± 0.07	0.03 ± 0.01	0.02 ± 0.01	0.16 ± 0.03	0.06 ± 0.03
	Expt.	0.96	0.02	0.00	0.02	
0.05	Simulation	0.80 ± 0.04	0.02 ± 0.01	0.01 ± 0.01	0.15 ± 0.02	0.02 ± 0.01

^aThis pathway is energetically closed at E_{rel} of 0.5 and 0.05 eV, and the reaction observed in the trajectories at these E_{rel} result from the incorrect use of reactant ZPE to promote reaction. ZPE also unphysically enhances reaction at 1.0 eV.

^b $[\text{CH}_3-\text{I}-\text{OH}]^-$ and $\text{CH}_2\text{I}^-(\text{H}_2\text{O})$ have the same mass-charge ratio and the experiments identify the ion as $\text{CH}_2\text{I}^-(\text{H}_2\text{O})$ or $\text{CH}_3\text{I}(\text{OH}^-)$.

^c E_{rel} 's for simulation are in normal text, E_{rel} 's for experiment are in parentheses.

In interpreting the experimental finding of this similar statistical/isotropic scattering for the $\text{CH}_3\text{OH} + \text{I}^-(\text{H}_2\text{O})$ and $\text{CH}_3\text{OH} + \text{I}^- + \text{H}_2\text{O}$ products, it was suggested that these dynamics result from trapping in the post-reaction complex $(\text{H}_2\text{O})\text{CH}_3\text{OH}---\text{I}^-$ for the $\text{S}_{\text{N}}2$ reaction.¹⁹ However, trapping in this complex is found to be unimportant in the simulations and, instead, the statistical/isotropic scattering arises from indirect mechanisms, which involve pre-reaction complexes and dynamics. Similar statistical/isotropic dynamics, without post-reaction complex formation, was also found for the $\text{Cl}^- + \text{CH}_3\text{I}$ $\text{S}_{\text{N}}2$ reaction.⁵⁸

A comparison of the experimental and simulation fractions of the proton transfer ions CH_2I^- or $\text{CH}_2\text{I}^-(\text{H}_2\text{O})$ is given in Figure 10(b). In the simulations there are three product ions with the 159 mass-charge ratio, i.e., $\text{HOH}---\text{CH}_2\text{I}^-$, $[\text{CH}_3-\text{I}-\text{OH}]^-$, and $\text{CH}_3\text{OH}---\text{I}^-$, which are not distinguished in the experiments. All three of these ions are included in the simulation $\text{CH}_2\text{I}^-(\text{H}_2\text{O})$ fractions. For both the CH_2I^- and $\text{CH}_2\text{I}^-(\text{H}_2\text{O})$ fractions there is good agreement between the experiment and simulation. Below 1.0 eV, the pathway for

CH_2I^- is energetically closed and the only feasible products are the $\text{CH}_2\text{I}^-(\text{H}_2\text{O})$ ions.

C. Dynamics of the H_2O molecule

It is of interest to study the dynamics of the H_2O molecule for the $\text{OH}^-(\text{H}_2\text{O}) + \text{CH}_3\text{I}$ $\text{S}_{\text{N}}2$ reaction. The statistical model, with equilibrium microsolvation, is that the H_2O molecule continues to interact with the reactive system during the course of the $\text{S}_{\text{N}}2$ reaction, forming $\text{I}^-(\text{H}_2\text{O})$ and/or $\text{CH}_3\text{OH}(\text{H}_2\text{O})$ which may receive sufficient energy to ultimately dissociate. As shown in Figure 2, the potential minima possibly affecting the $\text{S}_{\text{N}}2$ reaction are the complexes $(\text{H}_2\text{O})\text{HO}^----\text{HCH}_2\text{I}$ and $\text{CH}_2\text{I}^----\text{H}_2\text{O}(\text{H}_2\text{O})$ and post-reaction complex $(\text{H}_2\text{O})\text{CH}_3\text{OH}---\text{I}^-$. Trapping in these minima and forming complexes do not occur for the direct rebound and stripping mechanisms.

The probabilities of the above complexes participating in the $\text{S}_{\text{N}}2$ reaction are given in Table VI for the different E_{rel} . Also included are the probabilities for forming the product complexes $\text{I}^-(\text{H}_2\text{O})$, $\text{CH}_3\text{OH}(\text{H}_2\text{O})$, and $[\text{CH}_3-\text{I}-\text{OH}]^-(\text{H}_2\text{O})$.

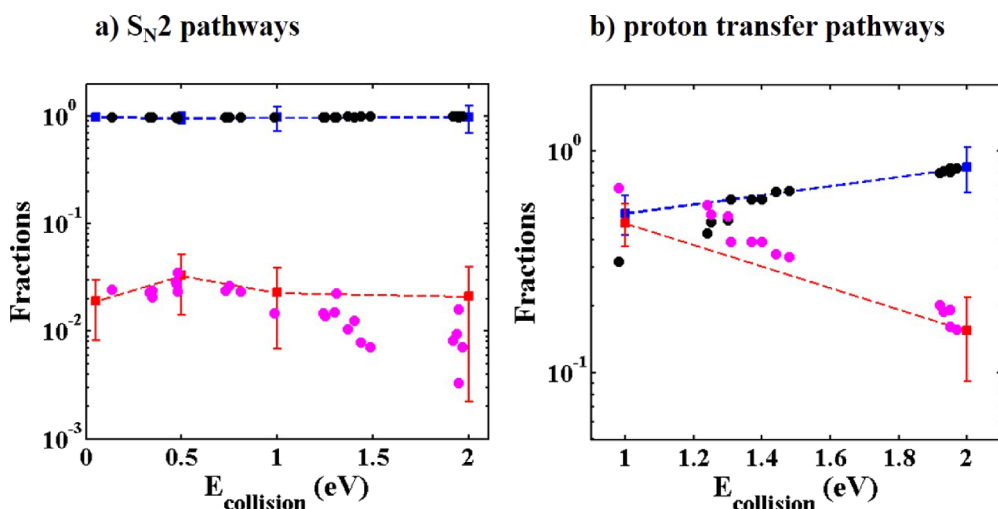


FIG. 10. (a) Fractional abundance of the solvated $\text{I}^-(\text{H}_2\text{O})$ products and of the I^- products as a function of collision energy: blue square, I^- fraction from simulation; black circle, I^- fraction from experiments; red square, $\text{I}^-(\text{H}_2\text{O})$ fraction from simulation; blue circle, $\text{I}^-(\text{H}_2\text{O})$ fraction from experiments. (b) Fractional abundance of the solvated $\text{CH}_2\text{I}^-(\text{H}_2\text{O})$ products and of the CH_2I^- products as a function of collision energy: blue square, CH_2I^- fraction from simulation; black circle, CH_2I^- fraction from experiments; red square, $\text{CH}_2\text{I}^-(\text{H}_2\text{O})$ fraction from simulation; blue circle, $\text{CH}_2\text{I}^-(\text{H}_2\text{O})$ fraction from experiments.

TABLE VI. Probabilities of complex formation with H₂O for the OH⁻(H₂O) + CH₃I → CH₃OH + I⁻ + H₂O S_N2 reaction.

Complex	E_{rel} (eV)	2.0	1.0	0.5	0.05
(H ₂ O)HO ⁻ --HCH ₂ I	0.02 ± 0.02	0.10 ± 0.07	0.58 ± 0.09	0.74 ± 0.09	
CH ₂ I ⁻ --H ₂ O(H ₂ O)	0.03 ± 0.03	0.06 ± 0.06	0.11 ± 0.03	0.10 ± 0.03	
(H ₂ O)CH ₃ OH--I ⁻	0.01 ± 0.01	0.01 ± 0.01	
[CH ₃ --I--OH] ⁻ (H ₂ O)	0.01 ± 0.01	0.02 ± 0.01	
I ⁻ (H ₂ O)	0.07 ± 0.04	0.04 ± 0.03	0.01 ± 0.01	0.03 ± 0.02	
CH ₃ OH(H ₂ O)	0.04 ± 0.03	0.02 ± 0.02	

For E_{rel} of 2.0 and 1.0 eV, complex formation with H₂O attached is unimportant. The probability is largest for the (H₂O)HO⁻--HCH₂I pre-reaction complex at 1.0 eV, but it is only 0.10 ± 0.07. Pre-reaction complex formation becomes important at E_{rel} of 0.5 and 0.05 eV, where 0.58 and 0.74 of the S_N2 trajectories form the (H₂O)HO⁻--HCH₂I pre-reaction complex, respectively. Ten percent of the trajectories form the proton transfer complex CH₂I⁻--H₂O(H₂O) at these energies. Formation of the S_N2 post-reaction complex (H₂O)CH₃OH--I⁻ is unimportant.

An approach for investigating the involvement of the H₂O molecule in the S_N2 reaction is to consider the time it leaves (i.e., dissociates from) the reactive system. This information is given in Figure 11, where the time H₂O leaves is given as a scatter plot versus the time the S_N2 product CH₃OH is formed.

Plots are given for the direct rebound, direct stripping, and indirect mechanisms. For E_{rel} of 2.0 and 1.0 eV, the preferential dynamics for the direct mechanisms is for H₂O to leave as CH₃OH is formed; i.e., H₂O departure is simultaneous with OH⁻ displacement of I⁻ for the S_N2 reaction. For the two lower E_{rel} , departure of H₂O after CH₃OH is formed becomes important for the direct mechanisms. For most of these events, H₂O is dissociating from I⁻ and not CH₃OH. Dissociation of H₂O from OH⁻(H₂O) before the S_N2 reaction occurs is similar to the ligand switching mechanism proposed by Viggiano and co-workers,⁵⁹ i.e., OH⁻(H₂O) + CH₃I → HO⁻--HCH₂I + H₂O.

For the indirect mechanisms, departure of H₂O from the reactive system before CH₃OH is formed becomes important. At 2.0 eV, for only approximately 10% of the indirect trajectories does H₂O leave as CH₃OH is formed. For this energy,

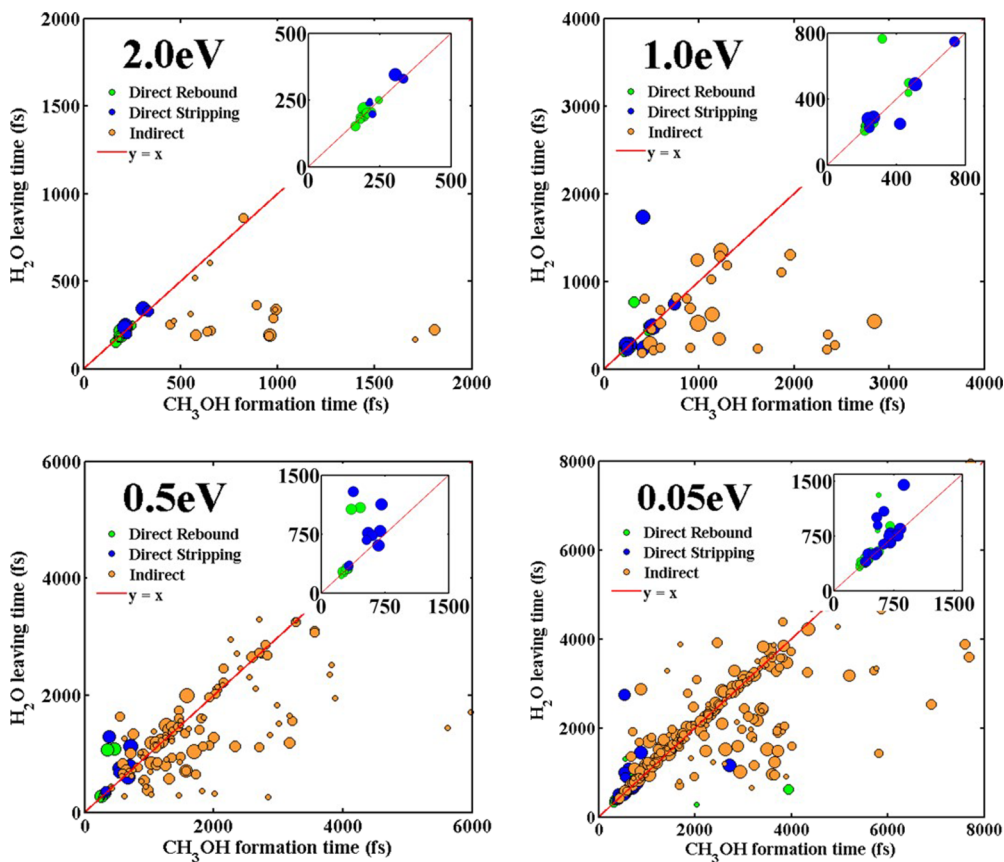


FIG. 11. Scatter plot of H₂O-leaving time versus CH₃OH-formation time for the OH⁻(H₂O) + CH₃I → CH₃OH + I⁻ + H₂O S_N2 reaction at different E_{rel} . Different atomistic mechanisms are distinguished: green circle for direct rebound, blue circle for direct stripping, and orange circle for indirect mechanisms.

the indirect trajectories are roundabout events and H₂O departs early. For the lower E_{rel} , where complex formation dominates the indirect mechanisms, the percentage of the trajectories increases for which H₂O departure and CH₃OH formation are nearly simultaneous. With a time width of ± 125 fs, about the line of unit slope, this percentage becomes 41%, 44%, and 41% for E_{rel} of 1.0, 0.5, and 0.05 eV, respectively. With a time width of ± 250 fs these percentages are 51%, 53%, and 52%. Thus, as E_{rel} is lowered, the H₂O molecule interacts with the reactive system for a longer period of time for the indirect mechanisms, and the probability that it dissociates from the reactive system as CH₃OH is formed increases.

VI. SUMMARY

The simulations reported here provide detailed atomistic dynamics for the microsolvated OH⁻(H₂O) + CH₃I reaction at collision energies of 2.0, 1.0, 0.5, and 0.05 eV. Comparisons are made with previous simulations of the unsolvated OH⁻ + CH₃I reaction and experiments for the OH⁻(H₂O) + CH₃I reaction. Of particular interest are the dynamics found for the solvating H₂O molecule.

At all collision energies, the dominant reaction pathway found from the simulations for the OH⁻(H₂O) + CH₃I reaction is formation of the S_N2 products CH₃OH + I⁻ + H₂O. The proton transfer pathway CH₂I⁻ + 2H₂O is of next importance at E_{rel} of 2.0 eV, but is energetically closed at the lower E_{rel} of 0.5 and 0.05 eV. At E_{rel} of 1.0 eV and lower, the second most important pathway involves formation of the ion [CH₃--I--OH]⁻. The most energetically favoured pathway is formation of the solvated S_N2 product I⁻(H₂O), but its yield is much less than that of I⁻. Formation of solvated CH₂I⁻, i.e., CH₂I⁻(H₂O), is energetically feasible at 2.0, 1.0, and 0.5 eV, but its yield is less than that of [CH₃--I--OH]⁻, which has the same mass. The major difference between the reaction pathways for OH⁻(H₂O) + CH₃I, as compared to OH⁻ + CH₃I, is the significant suppression of the proton transfer pathway for the microsolvated reaction.

There are multiple atomic-level mechanisms for forming the I⁻ and I⁻(H₂O) S_N2 product ions for the OH⁻(H₂O) reactant. There are both rebound and stripping direct mechanisms, and indirect mechanisms. The most important indirect mechanisms are formation of the (H₂O)HO⁻--HCH₂I pre-reaction complex, the proton-exchange mediated complexation HO⁻--HCH₂I \leftrightarrow HOH--CH₂I⁻ with and without H₂O, the roundabout mechanism, and combination of these mechanisms. The very interesting double-inversion mechanism found for the F⁻ + CH₃Cl S_N2 reaction⁶⁰ was not observed. The direct and indirect mechanisms are of similar importance at high E_{rel} for the OH⁻(H₂O) reactant, but the indirect mechanisms dominate at low E_{rel} . For the OH⁻ + CH₃I S_N2 reaction, the direct mechanisms are more important at all E_{rel} , and there are seven indirect mechanisms, as compared to 28 for OH⁻(H₂O) + CH₃I. At E_{rel} of 2.0 eV, the S_N2 cross section is statistically the same for OH⁻ and OH⁻(H₂O), but at 0.05 eV that for OH⁻(H₂O) is larger.

The scattering dynamics are different for the OH⁻ and OH⁻(H₂O) S_N2 reactions. For OH⁻, the stripping mechanism

with forward scattering dominates at E_{rel} of 2.0, 1.0, and 0.5 eV, but at 0.05 eV rebound and stripping have similar probabilities and the scattering becomes nearly isotropic. For OH⁻(H₂O), the convolution of the direct rebound and stripping and indirect mechanisms gives nearly isotropic scattering at each collision energy.

The probabilities for forming the product ions are very similar for the OH⁻(H₂O) + CH₃I simulations and experiments. For both, forming I⁻ is most important and I⁻(H₂O) least important. There is quantitative agreement between simulation and experiment for the relative yield of these two ions. As compared with experiment, for E_{rel} of 1.0, 0.5, and 0.05 eV, the simulations give an incorrect yield for the proton transfer product ion CH₂I⁻, which as described above results from the formation of products without ZPE for this pathway. The total reaction rate constant given by simulation for OH⁻ is ~ 2 times larger than that for OH⁻(H₂O) and both are in excellent agreement with experiment.^{25,57} The OH⁻(H₂O) + CH₃I CID cross section to form CH₃I + OH⁻ + H₂O is also in excellent agreement with experiment.²³

The experiment and simulation product energy partitioning for the OH⁻(H₂O) S_N2 reactions are in quantitative agreement. This includes the detailed dynamics for the solvated product ion I⁻(H₂O), where isotropic scattering is consistent with indirect/statistical dynamics. The indirect and isotropic dynamics for forming the S_N2 product ion I⁻ are similar to these for forming I⁻(H₂O).

A substantive difference in the experimental and simulation scattering for the OH⁻(H₂O) + CH₃I S_N2 reaction is in the velocity scattering angle distribution. In the experiments, backward scattering increases from 38% to 81% as E_{rel} is increased from 0.5 to 2.0 eV. For the simulations, the percentage of backward scattering remains at $\sim 50\%$ for each E_{rel} . The amount of the direct rebound mechanism found in the simulations increases with increase in E_{rel} , but it is not sufficient to enhance the backward scattering at high E_{rel} .

An important component of the OH⁻(H₂O) + CH₃I simulations is the dynamics found for the solvating H₂O molecule. As observed in the experiments, formation of the solvated ions I⁻(H₂O) and CH₂I⁻(H₂O) is not important. Temporary trapping in the S_N2 post-reaction complex is also not important. As found for the dynamics of other chemical reactions,^{13,14,24} the atomistic motions of the reactive system tend to not find these minima on the PES. Overall, the H₂O molecule leaves the reactive system before traversing the post-reaction region of the PES. For large E_{rel} , H₂O and the CH₃OH product preferentially leave the reactive system at the same time. As E_{rel} is decreased and indirect reaction becomes more important, the probability is enhanced for H₂O to depart before CH₃OH is formed.

The accuracy of the simulations reported here depends on the accuracy of the OH⁻(H₂O) + CH₃I PES given by the B97-1/ECP/d electronic structure theory used for the direct dynamics and the accuracy of classical mechanics for the chemical dynamics. As described above, overall, the simulations are in quite good agreement with experiment. The experimental property not correctly described by the simulations is the strong preference for backward scattering at the 2.0 eV collision energy. At such a high energy, this is not expected to be a shortcoming of classical dynamics. In future work, it will

be of interest to consider different electronic structure theories for the PES as was done in a recent S_N2 study.⁶¹

Inaccuracies in the classical dynamics are evident for events in which the reactant ZPE is used to form products where the reaction endothermicity exceeds the reactant energy. As a result, the product does not contain ZPE and should not be formed. These dynamics are found for the CH₂I⁻ + 2H₂O proton transfer products at 0.5 and 0.05 eV, the CH₂I⁻(H₂O) + H₂O proton transfer products at 0.05 eV, and the CH₃I + OH⁻ + H₂O CID products at 1.0, 0.5, and 0.05 eV. In addition, for CH₂I⁻ + 2H₂O proton transfer at 1.0 eV and CH₂I⁻(H₂O) + H₂O proton transfer at 0.5 eV, for which the reactant energy is only in slight excess of the reaction endothermicity, there are also inaccuracies in the dynamics. For CH₂I⁻ + 2H₂O proton transfer at 1.0 eV the reaction observed is unphysical, since the total vibrational energy of CH₂I⁻ + 2H₂O is less than the ZPE for each of the trajectories. These dynamics, with unphysical utilization of ZPE, are facilitated by the formation of pre-reaction complexes such as (H₂O)HO⁻---HCH₂I in Figure 2. With formation of such complexes, ZPE may transfer between all the rotation and vibration internal degrees of freedom, allowing reaction to occur in accord with the classical potential energy barrier without ZPE in the reaction products.⁵⁵ In contrast, formation of reaction products without ZPE is unimportant for the exothermic S_N2 pathways, and the proton transfer and CID pathways, at collision energies much higher than their endothermicities.

Models have been proposed and used for addressing the unphysical flow of ZPE in classical chemical dynamics simulations. One approach is to constrain either the total ZPE⁶² or individual mode ZPEs.⁶³⁻⁶⁵ For bimolecular reactions, trajectories which do not have ZPE in the reaction products are often discarded.⁶⁶⁻⁶⁸ This may be either a soft or hard ZPE constraint,^{69,70} where the soft constraint discards trajectories if the sum of the two products' vibrational energies is less than the sum of their ZPEs, whereas the hard constraint discards trajectories if either product has less vibrational energy than its ZPE. For the simulation results presented here, ZPE constraints have not been used to correct the OH⁻(H₂O) + CH₃I bimolecular dynamics. The results affected by unphysical ZPE dynamics are identified as described above. For the direct reactions, a soft or hard ZPE constraint, as described above, may be appropriate. But the applicability of such constraints is somewhat uncertain for bimolecular reactions mediated by pre-reaction complex formation as found here. We are currently investigating ZPE constraint models which incorporate pre-reaction complexes for bimolecular reactions.

The simulation results reported here, and their comparisons with experiment, have expanded our knowledge of S_N2 reactions and the role of microsolvation, and a deeper understanding of when classical chemical dynamics may be used to accurately study chemical reactions. In future simulations of the OH⁻(H₂O) + CH₃I reaction, there are a number of important questions to consider: e.g., why are indirect mechanisms much more important for OH⁻(H₂O) as compared to OH⁻; why does OH⁻(H₂O) have four times more indirect atomistic mechanisms than OH⁻; and why is the rebound mechanism less important for OH⁻ as compared to OH⁻(H₂O).

ACKNOWLEDGMENTS

The direct dynamics simulations reported here are based upon work supported by the Robert A. Welch Foundation under Grant No. D-0005. The simulations were performed on the Robinson cluster of the Department of Chemistry and Biochemistry at Texas Tech University. The experimental work was supported by the Deutsche Forschungsgemeinschaft under Contract No. WE2592/3-2. Rico Otto acknowledges support by the Landesgraduiertenförderung Baden-Württemberg. We thank the University of Freiburg for providing facilities and support for the measurements presented here. The authors also wish to acknowledge important collaborations with the Al Viggiano research group.

- ¹D. K. Bohme and G. I. Mackay, *J. Am. Chem. Soc.* **103**, 978 (1981).
- ²J. Chandrasekhar, S. F. Smith, and W. L. Jorgensen, *J. Am. Chem. Soc.* **106**, 3049 (1984).
- ³A. A. Viggiano, S. T. Arnold, R. A. Morris, A. F. Ahrens, and P. M. Hierl, *J. Phys. Chem.* **100**, 14397 (1996).
- ⁴J. V. Seeley, R. A. Morris, and A. A. Viggiano, *J. Phys. Chem. A* **101**, 4598 (1997).
- ⁵K. Doi, E. Togano, S. S. Xantheas, R. Nakanishi, T. Nagata, T. Ebata, and Y. Inokuchi, *Angew. Chem., Int. Ed.* **52**, 4380 (2013).
- ⁶Y. J. Cho, S. R. Vande Linde, L. Zhu, and W. L. Hase, *J. Chem. Phys.* **96**, 8275 (1992).
- ⁷L. Sun, W. L. Hase, and K. Song, *J. Am. Chem. Soc.* **123**, 5753 (2001).
- ⁸P. Manikandan, J. Zhang, and W. L. Hase, *J. Phys. Chem. A* **116**, 3061 (2012).
- ⁹J. P. Bergsma, B. J. Gertner, K. R. Wilson, and J. T. Hynes, *J. Chem. Phys.* **86**, 1356 (1987).
- ¹⁰B. J. Gertner, K. R. Wilson, and J. T. Hynes, *J. Chem. Phys.* **90**, 3537 (1989).
- ¹¹S. C. Tucker and D. G. Truhlar, *J. Am. Chem. Soc.* **112**, 3347 (1990).
- ¹²B. J. Gertner, R. M. Whitnell, K. R. Wilson, and J. T. Hynes, *J. Am. Chem. Soc.* **113**, 74 (1991).
- ¹³L. Sun, K. Song, and W. L. Hase, *Science* **296**, 875 (2002).
- ¹⁴J. G. López, G. Vayner, U. Lourderaj, S. V. Addepalli, S. Kato, W. A. deJong, T. L. Windus, and W. L. Hase, *J. Am. Chem. Soc.* **129**, 9976 (2007).
- ¹⁵S. Raugei, G. Cardini, and V. Schettino, *J. Chem. Phys.* **114**, 4089 (2001).
- ¹⁶M. Pagliai, S. Raugei, G. Cardini, and V. Schettino, *J. Mol. Struct.: THEOCHEM* **630**, 141 (2003).
- ¹⁷R. Otto, J. Xie, J. Brox, S. Trippel, M. Stei, T. Best, M. Siebert, W. Hase, and R. Wester, *Faraday Discuss.* **157**, 41 (2012).
- ¹⁸R. Otto, J. Brox, S. Trippel, M. Stei, T. Best, and R. Wester, *Nat. Chem.* **4**, 534 (2012).
- ¹⁹R. Otto, J. Brox, S. Trippel, M. Stei, T. Best, and R. Wester, *J. Phys. Chem. A* **117**, 8139 (2013).
- ²⁰M. Henchman, J. F. Paulson, and P. M. Hierl, *J. Am. Chem. Soc.* **105**, 5509 (1983).
- ²¹D. K. Bohme and A. B. Rakshit, *J. Am. Chem. Soc.* **106**, 3447 (1984).
- ²²P. M. Hierl, A. F. Ahrens, M. Henchman, A. A. Viggiano, J. F. Paulson, and D. C. Clary, *J. Am. Chem. Soc.* **108**, 3142 (1986).
- ²³P. M. Hierl, J. F. Paulson, and M. J. Henchman, *J. Phys. Chem.* **99**, 15655 (1995).
- ²⁴J. Xie, R. Sun, M. R. Siebert, R. Otto, R. Wester, and W. L. Hase, *J. Phys. Chem. A* **117**, 7162 (2013).
- ²⁵J. Xie, S. C. Kohale, W. L. Hase, S. G. Ard, J. J. Melko, N. S. Shuman, and A. A. Viggiano, *J. Phys. Chem. A* **117**, 14019 (2013).
- ²⁶H. Tachikawa, *J. Chem. Phys.* **125**, 133119 (2006).
- ²⁷R. Otto, *Dynamics of a Microsolvated Ion-Molecule Reaction* (Verlag Dr. Hut, 2011).
- ²⁸M. Valiev, E. J. Bylaska, N. Govind, K. Kowalski, T. P. Straatsma, H. J. J. Van Dam, D. Wang, J. Nieplocha, E. Apra, T. L. Windus, and W. A. de Jong, *Comput. Phys. Commun.* **181**, 1477 (2010).
- ²⁹R. G. Parr and W. Yang, *Density-Functional Theory of Atoms and Molecules* (Oxford University Press, 1989).
- ³⁰A. D. Becke, *J. Chem. Phys.* **107**, 8554 (1997).
- ³¹F. A. Hamprecht, A. J. Cohen, D. J. Tozer, and N. C. Handy, *J. Chem. Phys.* **109**, 6264 (1998).
- ³²J. Zhang and W. L. Hase, *J. Phys. Chem. A* **114**, 9635 (2010).
- ³³T. H. Dunning, *J. Chem. Phys.* **90**, 1007 (1989).

- ³⁴D. E. Woon and T. H. Dunning, *J. Chem. Phys.* **98**, 1358 (1993).
- ³⁵W. R. Wadt and P. J. Hay, *J. Chem. Phys.* **82**, 284 (1985).
- ³⁶W. P. Hu and D. G. Truhlar, *J. Phys. Chem.* **98**, 1049 (1994).
- ³⁷U. Lourderaj, R. Sun, S. C. Kohale, G. L. Barnes, W. A. de Jong, T. L. Windus, and W. L. Hase, *Comput. Phys. Commun.* **185**, 1074 (2014).
- ³⁸W. L. Hase, R. J. Duchovic, X. Hu, A. Komornicki, K. F. Lim, D. H. Lu, G. H. Peslherbe, S. R. Swamy, S. R. Vande Linde, A. Varandas, H. Wang, and R. J. Wolf, *Quantum Chem. Program Exch. (QCPE)* **16**, 671 (1996).
- ³⁹X. Hu, W. L. Hase, and T. Pirraglia, *J. Comput. Chem.* **12**, 1014 (1991).
- ⁴⁰G. H. Peslherbe, H. Wang, and W. L. Hase, *Adv. Chem. Phys.* **105**, 171 (1999).
- ⁴¹S. S. Xantheas, *J. Am. Chem. Soc.* **117**, 10373 (1995).
- ⁴²M. E. Tuckerman, D. Marx, M. L. Klein, and M. Parrinello, *Science* **275**, 817 (1997).
- ⁴³C. C. M. Samson and W. Klopper, *J. Mol. Struct.: THEOCHEM* **586**, 201 (2002).
- ⁴⁴A. B. McCoy, X. Huang, S. Carter, and J. M. Bowman, *J. Chem. Phys.* **123**, 064317 (2005).
- ⁴⁵J. M. Bowman, A. Kupperman, and G. C. Schatz, *Chem. Phys. Lett.* **19**, 21 (1973).
- ⁴⁶C. Schlier and A. Seiter, *J. Phys. Chem. A* **102**, 9399 (1998).
- ⁴⁷C. Schlier and A. Seiter, *Comput. Phys. Commun.* **130**, 176 (2000).
- ⁴⁸E. Lemmon, M. McLinden, D. Friend, P. Linstrom, and W. Mallard, *NIST Chemistry WebBook* (National Institute of Standards and Technology, Gaithersburg, 2011).
- ⁴⁹R. C. Weast, M. Astle, and W. Beyer, *CRC Handbook of Chemistry and Physics* (CRC Press, Inc., Boca Raton, FL, 1984).
- ⁵⁰R. Atkinson, D. Baulch, R. Cox, J. Crowley, R. Hampson, R. Hynes, M. Jenkin, M. Rossi, and J. Troe, *Atmos. Chem. Phys.* **4**, 1461 (2004).
- ⁵¹W. E. Farneth and J. I. Brauman, *J. Am. Chem. Soc.* **98**, 7891 (1976).
- ⁵²W. L. Hase, *Science* **266**, 996 (1994).
- ⁵³See supplementary material at <http://dx.doi.org/10.1063/1.4922451> for scan of the PES between the proton transfer pre-reaction complex ($\text{H}_2\text{O}^-\text{---HCH}_2\text{I}$) and post-reaction complex $\text{CH}_2\text{I}^-\text{---H}_2\text{O}(\text{H}_2\text{O})$, by varying the H-C distance.
- ⁵⁴J. Xie, M. McClellan, R. Sun, S. C. Kohale, N. Govind, and W. L. Hase, *J. Phys. Chem. A* **119**, 817 (2015).
- ⁵⁵W. L. Hase and D. G. Buckowski, *J. Comput. Chem.* **3**, 335 (1982).
- ⁵⁶J. Mikosch, S. Trippel, C. Eichhorn, R. Otto, U. Lourderaj, J. Zhang, W. Hase, M. Weidemüller, and R. Wester, *Science* **319**, 183 (2008).
- ⁵⁷A. A. Viggiano and P. M. Hierl, private communication (2014).
- ⁵⁸J. Zhang, U. Lourderaj, R. Sun, J. Mikosch, R. Wester, and W. L. Hase, *J. Chem. Phys.* **138**, 114309 (2013).
- ⁵⁹J. V. Seeley, R. A. Morris, A. A. Viggiano, H. Wang, and W. L. Hase, *J. Am. Chem. Soc.* **119**, 577 (1997).
- ⁶⁰I. Szabó and G. Czakó, *Nat. Commun.* **6**, 5972 (2015).
- ⁶¹R. Sun, C. J. Davda, J. Zhang, and W. L. Hase, *Phys. Chem. Chem. Phys.* **17**, 2589 (2015).
- ⁶²D. Bonhommeau and D. G. Truhlar, *J. Chem. Phys.* **129**, 14302 (2008).
- ⁶³J. M. Bowman, B. Gazdy, and Q. Sun, *J. Chem. Phys.* **91**, 2859 (1989).
- ⁶⁴W. H. Miller, W. L. Hase, and C. L. Darling, *J. Chem. Phys.* **91**, 2863 (1989).
- ⁶⁵G. Czakó, A. L. Kaledin, and J. M. Bowman, *J. Chem. Phys.* **132**, 164103 (2010).
- ⁶⁶J. C. Gray, D. G. Truhlar, L. Clemens, J. W. Duff, F. M. Chapman, Jr., G. O. Morrell, and E. F. Hayes, *J. Chem. Phys.* **69**, 240 (1978).
- ⁶⁷A. J. C. Varandas, *J. Chem. Phys.* **99**, 1076 (1993).
- ⁶⁸A. J. C. Varandas, *Chem. Phys. Lett.* **439**, 386 (2007).
- ⁶⁹G. Czakó, *J. Chem. Phys.* **138**, 134301 (2013).
- ⁷⁰G. Czakó, R. Liu, M. Yang, J. M. Bowman, and H. Guo, *J. Phys. Chem. A* **117**, 6409 (2013).